Yueyuan Jin

Numerical Modelling of Wave Overtopping Response to Sea Level Rise with REEF3D::SFLOW

Master's thesis in Coastal and Marine Engineering and Management
Supervisor: Hans Bihs
August 2020

Master's thesis

NTNU
Norwegian University of Science and Technology
Faculty of Engineering
Department of Civil and Environmental Engineering

NTNU
Norwegian University of
Science and Technology

Yueyuan Jin

Numerical Modelling of Wave Overtopping Response to Sea Level Rise with REEF3D::SFLOW

NTNU

Norwegian University of
Science and Technology

ERASMUS +: ERASMUS MUNDUS MOBILITY PROGRAMME

Master of Science in

COASTAL AND MARINE ENGINEERING AND MANAGEMENT

CoMEM

NUMERICAL MODELLING OF WAVE OVERTOPPING RESPONSE TO SEA LEVEL RISE WITH REEF3D::SFLOW

Norwegian University of Science and Technology
August 11, 2020

Yueyuan Jin

The Erasmus+: Erasmus Mundus MSc in Coastal and Marine Engineering and Management is an integrated programme including mobility organized by five European partner institutions, coordinated by Norwegian University of Science and Technology (NTNU).

The joint study programme of 120 ECTS credits (two years full-time) has been obtained at two or three of the five CoMEM partner institutions:

- Norges Teknisk- Naturvitenskapelige Universitet (NTNU) Trondheim, Norway
- Technische Universiteit (TU) Delft, The Netherlands
- Universitat Politècnica de Catalunya (UPC). BarcelonaTech. Barcelona, Spain
- University of Southampton, Southampton, Great Britain
- City University London, London, Great Britain

During the first three semesters of the programme, students study at two or three different universities depending on their track of study. In the fourth and final semester an MSc project and thesis has to be completed. The two-year CoMEM programme leads to a multiple set of officially recognized MSc diploma certificates. These will be issued by the universities that have been attended by the student. The transcripts issued with the MSc Diploma Certificate of each university include grades/marks and credits for each subject.

Information regarding the CoMEM programme can be obtained from the programme coordinator:

Øivind A. Arntsen, Dr.ing.
Associate professor in Marine Civil Engineering
Department of Civil and Environmental Engineering
NTNU Norway
Mob.: +4792650455 Fax: + 4773597021
Email: oivind.arntsen@ntnu.no

CoMEM URL: https://www.ntnu.edu/studies/mscomem

Disclaimer:
"The European Commission support for the production of this publication does not constitute an endorsement of the contents which reflects the views only of the authors, and the Commission cannot be held responsible for any use which may be made of the information contained therein."

CoMEM Thesis

This thesis was completed by:
Yueyuan Jin

Under supervision of:
Hans Bihs, Associate professor, NTNU
Weizhi Wang, Postdoctoral researcher, NTNU

As a requirement to attend the degree of
Erasmus+: Erasmus Mundus Master in Coastal and Marine Engineering and Management (CoMEM)

taught at the following educational institutions:

Norges Teknisk- Naturvitenskapelige Universitet (NTNU)
Trondheim, Norway

Technische Universiteit (TU) Delft
Delft, The Netherlands

At which the student has studied from August 2018 to August 2020.

Numerical Modelling of Wave Overtopping Response to Sea Level Rise with REEF3D::SFLOW

A Master Thesis
submitted to the Department of Civil and Transport Engineering
at the Norwegian University of Science and Technology

Master of Science

by

Yueyuan Jin

Abstract

Climate change has been a major topic in the research field recently because it influences the living environment of human-being. In the coastal zone and low-lying area, climate change causes sea level rise, which brings potential danger to the local economy development and even human life risk. In regard, coastal defence structures such as breakwaters and dikes are the direct protection measures. Therefore the impact of sea level rise on coastal defence structures is worthy to study. This thesis focuses on the impact of sea level rise on the wave overtopping at coastal structures.

Traditional overtopping research is based on physical laboratory experiments. By summarizing laboratory experiments results, wave overtopping on typical structures are studied. However, the cost of physical experiments is huge and results are limited by laboratory space and resources. Nowadays, with the updated computer hardware and improvement of computational fluid dynamics technology, numerical simulation method has been widely applied to wave overtopping topics.

In this thesis, an open-source hydrodynamics framework REEF3D is applied. The shallow water model REEF3D::SFLOW solves the shallow water equations with a quadratic non-hydrostatic pressure assumption. In order to solve the governing equations, the fifth-order weighted essentially non-oscillatory(WENO) finite difference scheme is applied to the convection term, and the third-order total variation diminishing(TVD) Runge-Kutta scheme is used as time advance format. Besides, as part of REEF3D framework, the computational fluid dynamics(CFD) module REEF3D::CFD solves the RANS equations. Due to the computational efficiency, REEF3D::SFLOW is used as the main research tool in the thesis study, while REEF3D::CFD is used for verification and inter-comparison.

Through different parameter combinations such as wave absorption methods and wave theories, the one-dimensional regular wave, two-dimensional regular wave, two-dimensional breaking wave and large-scale numerical wave tank model of coastal waves with topography changes are successfully simulated. The simulated wave surface results are compared with theoretical or experimental data to verify the validity of the numerical wave tanks. The results show consistency with theoretical or experimental values.

Besides, this thesis applies REEF3D::SFLOW to simulate wave propagation over

complex coastal structures. A numerical wave tank is established to study wave propagation and wave overtopping over a designed complex dike structure. By comparison with physical experimental measurements, the simulation results show that the simulated interaction between waves and complex structure is accurately. The calculated overtopping discharge from simulation results is also consistent with the measured value. Therefore, REEF3D::SFLOW is able to simulate wave propagation and wave overtopping over a complex dike structure. The study also demonstrates that the usage of validated numerical wave models such as REEF3D, is ideal for the investigation of future sea level rise scenarios.

Acknowledgments

This thesis is achieved to accomplish the degree requirement for a graduate student in the Erasmus Mundus Master program: Coastal and Marine Engineering and Management (CoMEM). I would like to take this opportunity to thank everyone who has helped me in the last two years.

Firstly, I would like to thank my main supervisor, Professor Hans Bihs. He gave guidance on my thesis from the topic selection to the main conception of the thesis. During this special period when the campus is closed due to coronavirus, Professor Hans supervised the progress of my thesis and offered me help.

Secondly, I would like to thank my co-supervisor, Weizhi Wang. During the writing of the thesis, he is very patient in answering my questions and guiding me through the whole process. I learn a lot about REEF3D from his explanations and suggestions.

Thirdly, I would also like to thank the CoMEM project coordinators in NTNU, Professor Oivind Arnesten and Sonja Hammer. They gave me great help in these two years. I appreciate all their encouragement to me.

I would also like to thank my CoMEM classmates and all my friends for their supports and friendship.

Last but not least, I would like to thank my family for their love all the time.

Contents

List of Figures

Chapter 1

Introduction

1.1 Background

Since the 1950s, people have observed the effects of climate change. With the development of science and technology, the use of fossil fuels has shown a rapid upward trend[16]. A large number of greenhouse gases are emitted into the atmosphere. This phenomenon makes the content of greenhouse gases in the atmosphere increase rapidly, causing global climate and ecological changes. In 2013, the Fifth Assessment Report(AR5) of the Intergovernmental Panel on Climate Change (IPCC) [16] demonstrated that human activities had caused the global climate to rise by 1 degree Celsius in the past 150 years[10]. The ocean plays a dominant role in climate-energy reserves. More than 90% of the net energy increased by global warming is stored in the ocean[21], and the increased heat causes the seawater to undergo thermal expansion. Combined with the action of land glaciers melting, the rate of sea level rise increases. Sea level changes have a profound impact on coastal areas. In some low-lying areas near the coastlines, changes in sea level threat human activities and development.

Representative concentration pathway (RCP) is a series of integrated emission scenarios to predict climate change under human activities in the near future[16]. Meanwhile, it describes greenhouse gas, aerosol emissions and main component contents of the atmosphere[16]. It is an important parameter to study when predicting severe change in the population, social economy, science and land use in the future. The well-known RCPs consist of one high emission scenario RCP8.5, two medium emission scenarios RCP6.0 RCP4.5 and one low emission scenario RCP2.6. RCP8.5, the baseline scenario in the absence of any climate change policy intervention, describes the largest temperature rise, followed by RCP6.0 and RCP4.5. RCP2.6 is a scenario with very low concentrations of greenhouse gases. In the RCP2.6 scenario, changes in energy use lead to significant reductions in greenhouse gas emissions globally. The

Fifth Assessment Report also states the predictions on future sea level changes under different emission scenarios. From the year of 2081 to 2100, the global average sea level under RCP2.6 scenario rises by 0.26-0.55m, the global average sea level under RCP4.5 scenario rises by 0.32-0.63m, and the global average sea level under RCP8.5 scenario rises by 0.45-0.82m[17].

Although Norway is less at risk from sea level rise from the rest of the world, it is still a valuable study field for the coastal engineers. Norway locates in the north-west of Scandinavia in Northern Europe. It faces the Norweigian Sea on the west side and borders Sweden and Finland in the east. With a rugged and sophisticated coastline over 20,000 km[22], the chance of coastline erosion caused by floods and waves is minimal. In recent years, many industrial projects have been carried out in low-lying areas close to the coastline. For example, several industries are located in the Oslofjord area. Besides, as the well-known saying that there is seawater in the veins of Norwegians. Norwegians have always lived by the sea. Along the west coast of Norway, many cities and villages still keep fishing as their lifestyle. Sea level rise is a potential hazard in these low-lying coastal areas.

Therefore, sea level rise is an unignorable topic. Sea level rise has the potential to bring hazards to coastal defence structures, including dikes and dams. Several wave parameters influence the performance of coastal structures. For example, sea level rise increases the coastal water depth, which determines the design still water level for defence structure. In this case, some coastal defence structures that have been in operation for a long time may not work correctly under the new water depth. Besides, there is extensive evidence that shows a relation between sea level rise and wave over-topping at the coast area. For example, T. Prime states that sea level rise motives wave overtopping to have a bearing on the cost of coastal flood events[34]. This thesis focuses on the study of the impact of sea level rise on the wave overtopping.

Wave overtopping is a common phenomenon that happens when waves interact with coastal structures. When designing flood defence structures, overtopping is consid-ered because it may cause instability and damage to the structures[40]. The discharge of overtopping is an intuitive parameter to measure the degree of wave overtopping and to determine the crest height of coastal structures. In the case of applying in-sufficient crest parameter to coastal structure design, the excessive overtop will cause serious impact on the top and rear side of the coastal structure. This design flaws may cause immeasurable loss of property and even loss of human life. Therefore, an accurate estimation of overtopping is of considerable significance to the design of coastal structures and the study of seal level rise effect at the coastal area.

1.2 Objectives

The primary purpose of this thesis is to study wave and wave overtopping in conjunction with sea level rise. Traditional methods for studying wave and wave overtopping include physical laboratory experiment, field observation and numerical wave tank simulation. Among them, numerical simulation has the advantages of time-saving, economical and convenient operational. With the improvement of computer hardware, numerical wave tank simulations are widely applied in multiple research field. In this thesis, the hydrodynamics framework REEF3D developed by the Department of Civil and Transport Engineering of NTNU is used to simulate wave and wave overtopping. REEF3D utilizes the multi-core design commonly used by modern processors and makes use of parallel programming to improve simulation efficiency. Also, REEF3D is open-source, so researchers and students innovated the framework constantly. As part of the REEF3D framework, REEF3D::SFLOW is an ideal tool to simulate depth-averaged wave propagation, especially for non-hydrostatic shallow water model. Therefore, the primary tool for studying wave and wave overtopping by numerical wave tank simulation is REEF3D::SFLOW.

Before applying REEF3D::SFLOW to investigate wave overtopping, this thesis conducts a series of cases algorithm verification. The study verifies the accuracy of REEF3D::SFLOW by numerical simulations of a one-dimensional regular wave, two-dimensional regular wave, two-dimensional breaking wave, and large-scale wave propagation at Mehamn harbour. Next, this thesis applies REEF3D::SFLOW to simulate wave propagation over a complex dike structure. Simulation results are compared with experimental results to verify model validation. Finally, this thesis estimates the impact of sea level rise on the tested complex dike structure by simulating of predicting sea level in the future.

Chapter 2

Literature Review

2.1 Introduction to wave

Waves are fluctuations that occur when seawater is disturbed. When the water particle leaves the original equilibrium position, it experiences periodic motion. In this way, waves propagate in a specific direction through the rise and fall of the water surface. Waves can be categorized by different wave periods. In this thesis, the studied gravity waves have a period of 0.25 seconds to 30 seconds[9]. Gravity waves are essential factors for coastal design. Gravity waves can have enormous potential energy. For example, a wave with a wave height of 6m can cause problems for shipping, offshore exploration and nearshore fishing. In coastal engineering, such catastrophic waves often lead to the destruction of ports, inundation of land and erosion of the coastline. Therefore, the study of gravity waves is an essential subject in coastal engineering.

When gravity waves enter shallow water from deep water, various changes occur. The wave speed, wavelength, wave height, and wave direction changes according to the seabed changes and the energy balance, but the wave period is always the constant. This characteristic of waves provides convenience for studying the changes in wave propagation under different water depths. Due to topographic changes, water depth changes and the interaction of coastal structures, waves have main phenomena of shoaling, refraction, diffraction and wave breaking. These phenomena are observed in the verification cases in Chapter 4. Wave deformation is an essential basis for verifying the validation of numerical simulations.

Besides, waves can be categorised into regular waves and irregular waves. Le Mehaute divided regular wave into the linear wave and nonlinear wave[27]. Le Mehaute used two dimensionless parameters, H/gT^2 as ordinate axis and d/gT^2 as abscissa axis. These two parameters can be used to determine the applicability of different wave theories[27]. In this thesis, Figure2.1 provides convenience for selecting generation wave theory for the numerical simulation. In general, for waves with relatively small

wave steepness and deep water depth, linear wave theory can be applied. For waves with significant steepness, Stokes wave theory can be applied. Moreover, in the shallow water, Cnoidal wave theory and Solitary wave theory are proper.

Figure 2.1: Regions of validity for various wave theories
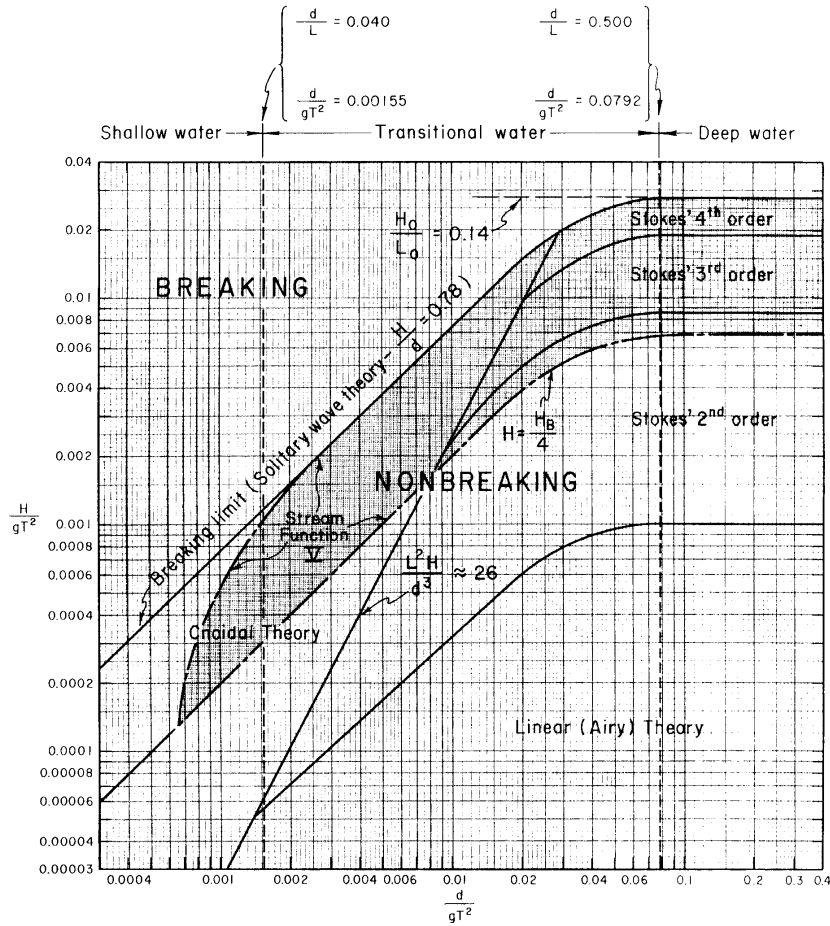
In this thesis, the wave height H is the vertical distance from the wave crest to wave trough. Wavelength and wave period T are the distance and time from one crest (or trough) to the next. The angular frequency ω and wave velocity c are related to other parameters as following:

$$\omega = \frac{2\pi}{T} \tag{2.1}$$

$$c = \frac{\lambda}{T} \tag{2.2}$$

5

Wavenumber is a characteristic of wave fluctuation by the definition of:

$$k = \frac{2\pi}{\lambda} \tag{2.3}$$

Different types of wave theories are applied to generate waves in REEF3D simulation. Generation wave theories can be linear wave theory, Stokes theory, Cnoidal wave theory, irregular wave theory, etc. In this thesis, there are three different wave theories applied in the simulation, the linear wave theory, the Stokes wave theory and the Cnoidal wave theory. Unlike the small-amplitude surface of linear waves, Stokes waves are nonlinear theory, allowing higher amplitudes. Cnoidal waves are shallow-water waves which wave surface has an elliptical cosine shape. Cnoidal wave theory close to the actual situation in reality in the shallow water.

As mentioned, the scope of linear wave theory is given by Le Mehaute in Figure 2.1. The limit of shallow water condition is $h/L¡0.05$ and the limit of the deepwater condition is $h/L¿0.5[9]$. Otherwise, the intermediate water depth condition applies. In this thesis, intermediate water depth condition, also know is the transitional water depth condition is applied in chapter 4. The wave profile of the intermediate water depth wave is:

$$\eta = \frac{H}{2} cos(kx - \omega t) \tag{2.4}$$

The Stokes wave theory assumes that water flow is a potential flow. The potential function is expressed by ϕ. The horizontal and vertical velocities are

$$u = \frac{\partial \phi}{\partial x} \tag{2.5}$$

$$w = -\frac{\partial \phi}{\partial z} \tag{2.6}$$

By assuming a small parameter perturbation ε to expand velocity potential and wave surface, M. Miche derived the second-order Stoke wave approximations[29]:

$$\phi = \varepsilon \phi_1 + \varepsilon^2 \phi_2 + \cdots \tag{2.7}$$

$$\eta = \varepsilon \eta_1 + \varepsilon^2 \eta_2 + \cdots \tag{2.8}$$

The second-order potential function and surface elevation solution are:

$$\phi = \frac{\pi H}{kT} \frac{\cosh[k(z+h)]}{\sinh(kh)} \sin(kx - \sigma t) + \frac{3}{8} \frac{\pi^2 H}{kT} \left(\frac{H}{L}\right) \frac{\cosh[2k(z+h)]}{\sinh^4(kh)} \sin 2(kx - \sigma t) \tag{2.9}$$

$$\eta = \frac{H}{2} \cos(kx - \sigma t) + \frac{\pi H}{8} \left(\frac{H}{L}\right) \frac{\cosh(kh) \cdot [\cos(2kh) + 2]}{\sinh^3(kh)} \cos 2(kx - \sigma t) \tag{2.10}$$

When the water depth is shallow, the higher order of the Stoke wave theory may be huge. At this time, Cnoidal wave theory is one of the proper options for shallow water nonlinear wave theories[11].

In the first-order Cnoidal wave theory, the approximate solution of the wave surface equation is

$$\eta = z_s - h \tag{2.11}$$

$$z_s = z_t + H cn^2 \left[2K(\kappa) \left(\frac{x}{L} - \frac{t}{T} \right), \kappa \right] \tag{2.12}$$

$$z_t = h - H + \frac{16h^3}{3L^2} K(\kappa)[K(\kappa) - E(\kappa)] \tag{2.13}$$

where z_s is the distance from water bottom to wave surface, K is the complete elliptic integral of the first kind and E is the complete elliptic integral of the second kind[11]. Fenton proposed the fifth-order Cnoidal wave theory, and he also explained the differences when applying fifth-order Cnoidal wave theory and the fifth-order Stoke wave theory[12].

2.2 Introduction to wave overtopping and sea level rise

Overtopping refers to water over the top of the structure during the interaction of waves and structures[40]. Studying the volume of overtopping and the interaction of waves with structure can better help engineers design coastal buildings. At present, most of the research on wave overtopping are based on laboratory physics models. Saville (1955) conducted small-scale laboratory experiments for regular wave overtopping rate and runup height[36]. Based on the analysis of experiment data, he proposed averaged overtopping volume formula and his study enlightened later researchers. Yuichi and Akira (1965) proposed the influence of different water depths and different wave heights towards wave overtopping[18]. Weggel (1977) summarized the study of Saville and proposed new equations of wave overtopping over single layer slope structure[43]. Nowadays, empirical formulas of overtopping are popular for practical purposes. Owen (1980) proposed wave overtopping formulas that overtopping discharge decreases exponentially as the structure crest increases[33]. Van der Meer (1998) proposed average overtopping discharge and maximum overtopping discharge formulas based on a lot of experimental research work[39]. His formulas continuously update in recent years and are widely applied around Europe[40]. In

EurOtop Manual, an overtopping design manual based on European research, the general formulae for wave overtopping discharges is shown below[40]:

$$\frac{q}{\sqrt{gH_{m0}^3}} = a \exp\left(-b\frac{R_c}{H_{m0}}\right) \tag{2.14}$$

where q is the average wave overtopping discharge, R_c is crest freeboard, H_m0 is the spectral significant wave height, a and b are fitted coefficient.

The formula is developed by different design of defence structure. For example, the wave overtopping at shallow slope foreshores can be described by the following developed formula:

$$\frac{q}{\sqrt{g \cdot H_{m0}^3}} = 10^{-0.79} \cdot \exp\left(-\frac{R_c}{\gamma_f \cdot \gamma_\beta \cdot H_{m0} \cdot (0.33 + 0.022 \cdot \xi_{m-1,0})}\right) \tag{2.15}$$

where γ_f is the influence factor for roughness elements on a slope, γ_β is the influence factor for oblique wave attacking on structure, $\xi_{m-1,0}$ is the wave steepness.

As can be seen, the empirical formulas are experimentally based and are hardly appliable to a complex structure. The method to study the overtopping over intricate structure is mainly through physical experiments, and there are some attempts to combine numerical simulation methods with physical experiments.

Besides, as seen from the general formula, structure crest is impoartant factor that affact overtopping. Structure crest is affected by wave parameters and water depth. Rising sea levels by global warming must take into account in the future design of coastal structures. EurOtop predicts a sea level rise of 0.2m to more than 1,0m in the coming next 100 years and it prescribes related standards about sea level rise in overtopping design[40]. Certain sea level rise level should be taken into account, but the range can be different prescribed by countries. According to various types of structures, such as structural complexity, the return period of sea level rise may be different. A simple design structure, such as earth dikes can be easily rebuilt to increase structure crest. Therefore a sea level rise with 50 years return period for a relatively simple design is sufficient. Complex structures such as concrete breakwaters are lack of flexibility and hardly be rebuilt[40]. Therefore a more extended return period 100 years or more for sea level rise is required[40].

2.3 Introduction to numerical wave tank simulation

Nowadays, the numerical wave tank model constructed by wave theory is gradually replacing the physical experiments in the laboratory. Based on the development of computational fluid dynamics, great many numerical wave tank models have been applied to scientific research and commercial applications. In reality, waves are affected by objective conditions such as structures and topography and result in breaking and eddying. Therefore, selecting the appropriate numerical model according to the wave characteristic helps to obtain a more reliable result.

Several common methods for constructing numerical wave tank include finite volume method, finite element method and boundary element method.

Since the Navier-Stokes equation is a typical equation used to describe classical fluid dynamics. Therefore, the finite difference based method is applied to solve the Navier-Stokes equation. This method needs proper grid precision to ensure the accuracy of numerical values, so it is limited by computer hardware and efficiency of computation. In 1976, Longuet-Higgins and Cokelete used the coupled finite element and boundary element to simulate the phenomenon of wave breaking in unbounded regions[28]. At the moment, they introduced the boundary element method to the numerical wave tank technology. In 1978, Harten and Efrony divided the object water columns into the separate tanks and simulated more accurate results, by this means they improved the boundary element method[14]. In 1995, P. Wang studied the long-term evolution of nonlinear waves according to the boundary element method and effectively improved the calculation efficiency of this method[41].

In 1981, Hirt and Nichois published a paper about the famous Volume of Fluid (VOF) method, which successfully simulated free surface motion of waves by combining the interface tracking method with the finite difference method[15]. Nowadays, there are great many numerical wave tank simulation software and CFD solvers for researchers and students to use. For example, simulations of gravity wave flow can be achieved by OpenFOAM[13] solver and FEniCS[26] solver. The former deals with the governing equation and complex geometric shapes according to the Finite volume method. Meanwhile, OpenFOAM contains a large number of solvers, and researchers can also independently write their solvers, which has a wide range of applications. The latter FEniCS deals with the application model according to the Finite Element Method to solve partial differential equations.

The numerical simulation method for wave overtopping has also attracted researchers' attention. The commonly used numerical model to solve wave overtopping is composed of nonlinear shallow water equation with the Navier-Stokes equation. The numerical model based on the shallow water equation has high efficiency and stable

operation. Therefore it is widely used in the field and has remarkable achievements. N. Kobayashi used nonlinear shallow water equation to simulate the overtopping of a slope embankment in 1989[31]. In 2003, A. Soliman[38] numerally simulated overtopping of irregular waves using Reynolds-averaged Navier-Stokes equations. Today, many CFD software and solvers can emulate wave overtopping process, such as Open-FOAM. The method of simulating overtopping with the numerical model has been applied widely in coastal engineering and research application.

Besides, wave models based on the Boussinesq equation has been widely applied in the research recently. With the development of computer technology, the Boussinesq equation has gradually become an newly ideal model among others describing waves in shallow water[24]. Now, the Boussinesq equations have developed into a class of equations; they all have two critical parameters, namely ε and μ^2. ε is the ratio of wave amplitude to water depth in order to measure wave nonlinearity. μ^2 is the square of the ratio of water depth to wavelength, which is to measure the dispersion of waves. The classic Boussinesq equation is only suitable for simulating weakly nonlinear and weakly dispersive waves under the same order of ε and μ^2. This scenario is not always the truth in reality. When the wave propagates from deep water to shallow water, as the water depth decreases, the nonlinearity of the wave will gradually increase, and higher-order harmonics with shorter wavelengths will appear. Therefore, the classical Boussinesq equation will produce more substantial errors when simulating waves with strong nonlinearity and waves with shorter wavelengths and larger water depths.

There are two ways to improve the Boussinesq equation. One is to retain more high-order terms in the derivation process. For example, P. A. Madsen has proposed a series of even fourth-order high-order Boussinesq equations[24]. However, the high-order equations will cause a significant increase amount in calculations and a longer simulation time. Another method is to artificially introduce some dispersion phases into the classical equations to improve the dispersion accuracy of the equations, for example P. A. Madsen[23]. Besides, A. Jeschke [19] proposed the method of applying secondary pressure to the vertical pressure profile. This method avoids the numerical instability caused by the Boussinesq model in higher-order terms and does not excessively increase the simulation time and operating cost. The above methods are applied in the REEF3D::SFLOW when the shallow water equations are derived.

REEF3D is a continuously updated hydrodynamic framework for applications in many fields, such as coastal engineering, environmental engineering, and marine engineering. As an open-source framework, it is innovative for researchers and students. REEF3D frame contains many subframes that can solve various types of engineering problems. For example, in coastal engineering, REEF3D::CFD can simulate wave interaction with different types of coastal structures. A. Aggarwal applied REEF3D::CFD to the research of breaking wave interaction with a jacket structure in 2019[2]. In the same year, M. Alagan also involved the study of breaking wave

10

interaction with slender structures to REEF3D[6]. REEF3D::CFD also has excellent computing performance for complex free-surface flow. For example,N. Ahmad used REEF3D::CFD to free surface of scour around different types of structures[3], [4], [5]. The REEF3D subframe can simulate sediment transport, such as bedload transport and suspended load transport. M.S. Afzal simulates the 3D model of sediment transport under the combined action of wave and current with REEF3D sediment transport module[1]. REEF3D also has research applications in ocean engineering. T. Martin simulated the moored-floating structure model with REEF3D[25].

REEF3D::SFLOW is applied as a shallow water model. W. Wang's research on the combination of shallow water equation with quadratic pressure approximation[42] has provided strong theoretical knowledge and inspiration for the application of REEF3D::SFLOW in this thesis. Therefore, this thesis uses REEF3D as the primary tool to simulate wave propagation.

Chapter 3

Numerical Model

REEF3D has a wide range of applications in the field of marine and coastal engineering. This framework can successfully solve the problems of the complex free surface, open channel flow, numerical wave tank and sediment transport. The code is written in C++ language with MPI, an open-source, high-performance computation standard. REEF3D uses high-order finite-difference, and Cartesian grids with ghost cell immersed boundary method to process the object surface[8]. At the same time, it uses the phase-resolved wave model to calculate detailed free surface phenomena through time-domain analysis.

This chapter briefly introduces the characteristics of the numerical simulation REEF3D and its basic theoretical methods.

3.1 REEF3D::CFD governing equations

In the wave numerical simulation method, the compressibility of water flow is generally not considered and water is treated as an incompressible viscous fluid. REEF3D uses Navier-Stokes equations to control fluid movement. Navier-Stokes equations describe the equations of motion for the conservation of momentum of viscous incompressible fluids, also referred to as N-S equations[9]. Reynolds-averaged Navier-Stokes equations are based on turbulent flows. Turbulence flows assume that the flow field variable in turbulence is composed of time-averaged and fluctuating quantities, from which the N-S equation can be treated to obtain the Reynolds-averaged Navier-Stokes equation (RANS equation for short). In this thesis, incompressible RANS equations are selected, and the expressions are:

$$\frac{\partial u_i}{\partial x_i} = 0 \tag{3.1}$$

$$\frac{\partial u_i}{\partial t} + u_j \frac{\partial u_i}{\partial x_j} = -\frac{1}{\rho}\frac{\partial p}{\partial x_i} + \frac{\partial}{\partial x_j}\left[\nu\left(\frac{\partial u_i}{\partial x_j} + \frac{\partial u_j}{\partial x_i}\right) - \overline{u_i u_j}\right] + g_i \tag{3.2}$$

where u_i, u_j are time-averaged velocity, ρ is the water density, p is pressure, ν is the kinematic viscosity, g is gravity acceleration.

3.2 REEF3D::SFLOW governing equations

As part of REEF3D, SFLOW is developed as a non-hydrostatic shallow water model. When designing coastal structures, the local wave parameters need to be determined. Usually, the measured data are the wave parameters of the deep sea. Therefore, it is one of the goals of the engineers to determine the change of the simulated wave from deep water to shallow water. The shallow water model is the primary governing model for plane flow simulation calculation. It ignores the uneven vertical distribution of velocity, and it is sufficient to simulate a wide range of plane flow patterns such as bay currents and submerged dams. In coastal areas where the water depth is shallow, shallow water model is a useful tool to apply in the simulation.
In REEF3D::SFLOW, a stable flow satisfies the continuity equation of incompressible fluid:

$$\frac{\partial U}{\partial x} + \frac{\partial V}{\partial y} + \frac{\partial W}{\partial z} = 0 \tag{3.3}$$

Momentum transfer of ideal fluid can be described by Euler equations[42]:

$$\frac{\partial U}{\partial t} + U\frac{\partial U}{\partial x} + V\frac{\partial V}{\partial y} + W\frac{\partial W}{\partial z} = -\frac{1}{\rho}\frac{\partial P_T}{\partial x} \tag{3.4}$$

$$\frac{\partial V}{\partial t} + U\frac{\partial V}{\partial x} + V\frac{\partial V}{\partial y} + W\frac{\partial V}{\partial z} = -\frac{1}{\rho}\frac{\partial P_T}{\partial y} \tag{3.5}$$

$$\frac{\partial W}{\partial t} + U\frac{\partial W}{\partial x} + V\frac{\partial W}{\partial y} + W\frac{\partial W}{\partial z} = -\frac{1}{\rho}\frac{\partial P_T}{\partial z} - g \tag{3.6}$$

where U is velocity in x direction, V is the velocity in y direction, W is the velocity in z directions, ρ is the water density, P_T is total pressure, and g is gravity acceleration. In the shallow water model, the water depth h is the combination of the still water depth d and the free surface elevation ζ:

$$h = d + \zeta \tag{3.7}$$

The velocity vector along the horizontal direction is defined as:

$$\mathbf{U} = (U, V) \tag{3.8}$$

Kinematic conditions of free surface and bottom are as follows:

$$W|_\zeta = \frac{\partial \zeta}{\partial t} + \boldsymbol{U}|_\zeta \cdot \nabla \zeta \tag{3.9}$$

$$W|_{-d} = -\boldsymbol{U}|_{-d} \cdot \nabla d \tag{3.10}$$

As can be seen, the motion orbit of water particle in shallow water is elliptic. With the increase of water depth, the horizontal radius of the ellipse remains unchanged while the vertical radius decreases continuously. Therefore the horizontal acceleration is much larger than the vertical acceleration. Therefore, the pressure in the fluid is hydrostatic. Assume by the hydrostatic pressure of shallow water:

$$P_T = P + Q = \rho g(\zeta - z) + Q \tag{3.11}$$

where P_T is the total pressure, P is the hydrostatic part and Q is the hydrodynamic part.

Boundary condition of free surface is:

$$P_T|_\zeta = P|_\zeta = Q|_\zeta = 0 \tag{3.12}$$

REEF3D::SFLOW is also designed for averaged depth. The basic equation of two-dimensional flow in a plane with an average depth can be obtained by integrating the basic three-dimensional equation with average depth. The average velocities along the water depth are:

$$\mathbf{u} = (u, v) = \frac{1}{h} \int_{-d}^{\zeta} U dz \tag{3.13}$$

$$w = \frac{1}{h} \int_{-d}^{\zeta} W dz \tag{3.14}$$

The dynamic pressure along the water depth is:

$$q = \frac{1}{h} \int_{-d}^{\zeta} Q dz \tag{3.15}$$

A. Jeschke et al gives the equations of quadratic vertical pressure profile[19]:

$$P|_{-d} = \frac{3}{2} q + \frac{1}{4} \rho h \phi \tag{3.16}$$

$$\phi = -\nabla d \cdot (\partial_t \mathbf{u} + (\mathbf{u} \cdot \nabla \mathbf{u}) - \mathbf{u} \cdot \nabla(\nabla d)) \cdot \mathbf{u}_\leftarrow \tag{3.17}$$

Therefore, the governing equations of REEF3D::SFLOW are given:

$$\frac{\partial \zeta}{\partial t} + \frac{\partial hu}{\partial x} + \frac{\partial hv}{\partial y} = 0 \tag{3.18}$$

$$\frac{\partial u}{\partial t} + u\frac{\partial u}{\partial x} + v\frac{\partial u}{\partial y} = -g\frac{\partial \zeta}{\partial x} - \frac{1}{\rho h}\left(\frac{\partial hq}{\partial x} - \left(\frac{3}{2}q + \frac{1}{4}\rho h\phi\right)\frac{\partial d}{\partial x}\right) \tag{3.19}$$

$$\frac{\partial v}{\partial t} + u\frac{\partial v}{\partial x} + v\frac{\partial v}{\partial y} = -g\frac{\partial \zeta}{\partial y} - \frac{1}{\rho h}\left(\frac{\partial hq}{\partial y} - \left(\frac{3}{2}q + \frac{1}{4}\rho h\phi\right)\frac{\partial d}{\partial y}\right) \tag{3.20}$$

$$\frac{\partial w}{\partial t} + u\frac{\partial w}{\partial x} + v\frac{\partial w}{\partial y} = \frac{1}{\rho h}\left(\frac{3}{2}q + \frac{1}{4}\rho h\phi\right) \tag{3.21}$$

In REEF3D::SFLOW, W. Wang[42] from REEF3D Development Team uses the Poisson equation to describe formula containing pressure information:

$$\frac{h_p}{\rho}\left(\frac{\partial^2 q}{\partial x^2} + \frac{\partial^2 q}{\partial y^2}\right) + \frac{2q}{\rho h_p} = \frac{1}{\partial x \partial t}\left(-h_p\left(\frac{\partial u}{\partial x} + \frac{\partial v}{\partial y}\right) - 2w - u\frac{\partial d}{\partial x} - v\frac{\partial d}{\partial y}\right) \tag{3.22}$$

Where h_p is water level at the center of cell.

In W. Wang's research[42], Poisson pressure equation is solved by the solver library HYPRE with the PFMG-preconditioned BICGStab algorithm. With the solution of dynamic pressure, the velocity expressions in the staggered grid are solved under the quadratic pressure approximation.

3.3   Discretization of the convective terms

In the numerical simulation of complex fluid with discontinuities, the truncation error of the numerical method and the limitation of the algorithm on smooth characteristics lead to several problems. Problems such as order reduction at discontinuities and distortion in the capture of complex fluid motion are the difficulties. The study of weighted essential non-oscillatory scheme (WENO) has good progress. Liu [32] proposed WENO scheme format based on ENO format. The WENO scheme can keep the numerical solution of WENO scheme essentially non-oscillating near the discontinuity and obtain high order of accuracy in the smooth region. When ENO scheme has an accuracy order of r, the WENO scheme can achieve accuracy order of $2r - 1$. Therefore, WENO scheme is suitable for strong discontinuities and smooth situations.

Based on WENO scheme study, Jiang and Shu [20]proposed a new WENO scheme to obtain higher accuracy of the numerical solution. In this thesis, the spatial discrete format is the fifth-order WENO finite differential scheme proposed by Jiang[20], also

referred to as WENO5. Wang[42] gives the discretized form of REEF3D::SFLOW governing equation.

$$\frac{\zeta_i^{n+1} - \zeta_i^n}{\Delta t} + \frac{\hat{h}_{i+1/2}^n u_{i+1/2}^{n+1/2} - \hat{h}_{i-1/2}^n u_{i-1/2}^{n+1/2}}{\Delta x} = 0 \tag{3.23}$$

Where $i + 1/2$ is cell face and $\hat{h}_{i+1/2}$ is the water level at cell face $i + 1/2$. Wang[42] reconstructed with the WENO procedure:

$$\hat{h}_{i+1/2}^{\pm} = \omega_1^{\pm} \hat{h}_{i+1/2}^{1\pm} + \omega_2^{\pm} \hat{h}_{i+1/2}^{2\pm} + \omega_3^{\pm} \hat{h}_{i+1/2}^{3\pm} \tag{3.24}$$

Where w is smoothness indicators, h indicates ENO stencil , and $\pm$ indicates upwind direction. Smoothness indicators and ENO stencils are:

$$IS_1 = 13(h_{i-2} - 2h_{i-1} + h_i)^2 + 3(h_{i-2} - 4h_{i-1} + 3h_i)^2 \tag{3.25}$$

$$IS_2 = 13(h_{i-1} - 2h_i + h_{i+1})^2 + 3(h_{i+1} - h_{i-1})^2 \tag{3.26}$$

$$IS_3 = 13(h_i - 2h_{i+1} + h_{i+1})^2 + 3(3h_i - 4h_{i+1} + h_{i+1})^2 \tag{3.27}$$

$$\hat{h}_{i+1/2}^{1-} = \frac{1}{3}h_{i-2} - \frac{7}{6}h_{i-1} + \frac{11}{6}h_i \tag{3.28}$$

$$\hat{h}_{i+1/2}^{2-} = -\frac{1}{6}h_{i-1} + \frac{5}{6}h_i + \frac{1}{3}h_{i+1} \tag{3.29}$$

$$\hat{h}_{i+1/2}^{3-} = \frac{1}{3}h_i + \frac{5}{6}h_{i+1} - \frac{1}{6}h_{i+2} \tag{3.30}$$

3.4 Time step and time discretization

In this thesis, the time advance format is the third-order TVD Runge-Kutta format proposed by Shu[37]. Runge-Kutta method is a high-accuracy one-step algorithm widely used in the engineering industry. Third order TVD Runge-Kutta has expression of:

$$u^{n+1} = \frac{1}{3}u^n + \frac{2}{3}u^{(2)} + \frac{2}{3}\Delta t L\left(u^{(2)}\right) \tag{3.31}$$

In which

$$\begin{cases} u^{(2)} = \frac{3}{4}u^n + \frac{1}{4}u^{(1)} + \frac{1}{4}\Delta t L\left(u^{(1)}\right) \\ u^{(1)} = u^n + \Delta t L\left(u^n\right) \end{cases} \tag{3.32}$$

L(u) is discrete operator which describes by

$$\frac{\mathrm{d}u}{\mathrm{d}t} = L(u) \tag{3.33}$$

3.5   MPI for parallel computation

Most mainstream CPU manufacturers improve the performance of microprocessors by using parallel processing and improve the overall performance of processors by placing multiple relatively simple processors on the chip. Such integrated computers with multiple processors are called multi-core processors. In order to make the program take full advantage of the performance of multi-core processors, run faster and get more timely computation data, software development engineers rewrite serial programs into parallel programs. Parallel computing is done by assigning tasks to several processors. Each processor individually handles the assigned task. In this way, multiple processors can work on the same main task at the same time, thus reducing the amount of time the computer computing on tasks. At present, multi-core hardware such as quad-core CPU and six-core CPU in the market provide the hardware foundation for parallel computing. REEF3D is about dividing the simulation domain into smaller subdomains and using multi-core processors to compute simultaneously[7].

MPI (multipoint interface) is a model based on parallel computing, which can be understood as an extensible messaging model. In REEF3D, communication between subdomains is achieved through ghost cell, and MPI is used to exchange ghost cell values and thus realize communication on the boundaries of subdomains[7]. Using the ghost cell method of immersion boundary overcomes the limitation of the stability of small grids, and makes Cartesian grids more effectively dealing with the problems of complex geometric shapes.

3.6   Wave generation and absorption

REEF3D has options for different wave generation and absorption methods. The two methods used in this thesis are the relaxation method and the Dirichlet method.

The relaxation method was first used in wave elimination, and scholars found that the method could be applied to wave generation at the same time. The principle of relaxation method is to set up a wave-making region and a wave-eliminating region at the front and back ends of the numerical flume, which is equivalent to adding the inlet and outlet boundary conditions in the calculation region[7]. In the wave-making region, the waves are generated at the interface without any interference. The reflected waves are absorbed by the relaxation method. In the exit zone, the

wave is dissipated by a relaxation method to avoid the reflection from impressing the numerical results. Therefore, the relaxation method can ensure that the wave will not be affected by the secondary reflected and transmitted waves when it propagates in the numerical flume.

The relation formula of relaxation method is:

$$u_{\mathrm{r}} = R(x)u_{\mathrm{a}} + (1 - R(x))u_{\mathrm{c}} \tag{3.34}$$

$$\varphi_{\mathrm{r}} = R(x)\varphi_{\mathrm{a}} + (1 - R(x))\varphi_{\mathrm{c}} \tag{3.35}$$

Where R is the value of relaxation, a represents the analytical value and c represents the computational value.

$$R\left(x'\right) = 1 - \frac{\exp\left(x'^{3.5} - 1\right)}{\exp(1) - 1}, x' \in [0, 1] \tag{3.36}$$

Where x' present the length of the relaxation zone.

The Dirichlet method generates waves based on Dirichlet boundary conditions[35]. This method can be applied to a variety of laboratory wave generator. It is the most straightforward and feasible condition to analyze the velocity distribution of the free interface and the entire water column[35]. The wave generated by the Dirichlet method requires two variables in every time step. One is to generate the free surface level at the boundary, and the other is the selected preset speed, including horizontal and vertical components.

Compared to the relaxation method, Dirichlet method at the inlet and outlet has the advantages of reducing the computation domain and shortening calculation time. However, the relaxation method gives less influences of secondary reflected waves or transmitted waves.

3.7   Wave overtopping

In the physical model, the collection of the overtopping volume is achieved by setting a water container behind the structure. From wave running over the crest overtop for the first time until a specific time node, the water in the container is gathered. The overtopping discharge rate can be calculated as the following:

$$q = \frac{Q}{lt} \tag{3.37}$$

where q is the overtopping discharge rate per unit length, Q is the total overtopping volume in the container, l is the width of defence structure, t is the period of overtopping.

In this numerical simulation, overtopping is obtained by the flux of a vertical surface on the design wall as shown as the red box in Figure3.1. The flux surface can be understood as a surface of the cuboid area at the top of a dike structure. In the overtopping case simulation in chapter 5, the flux surface is located directly above the design wall. The bottom of the cuboid area is the same height as the top of the wall crest. The top of the cuboid area is the same height as the top of the numerical wave tank domain height. The thickness of the cuboid in the wave propagation direction is related to the time step Δt and simulation cell size Δx. Therefore, according to the difference between the water surface in the flux surface η and the crest of the building h_{crest}, the amount of wave crossing in each time step can be roughly calculated. The total amount of overtopping discharge can be roughly approximated through time integration over the simulation time T.

$$q = (\eta - h_{\text{crest}}) \times \frac{\Delta x}{\Delta t} \tag{3.38}$$

$$Q = \int_0^t q \times l \partial t \tag{3.39}$$
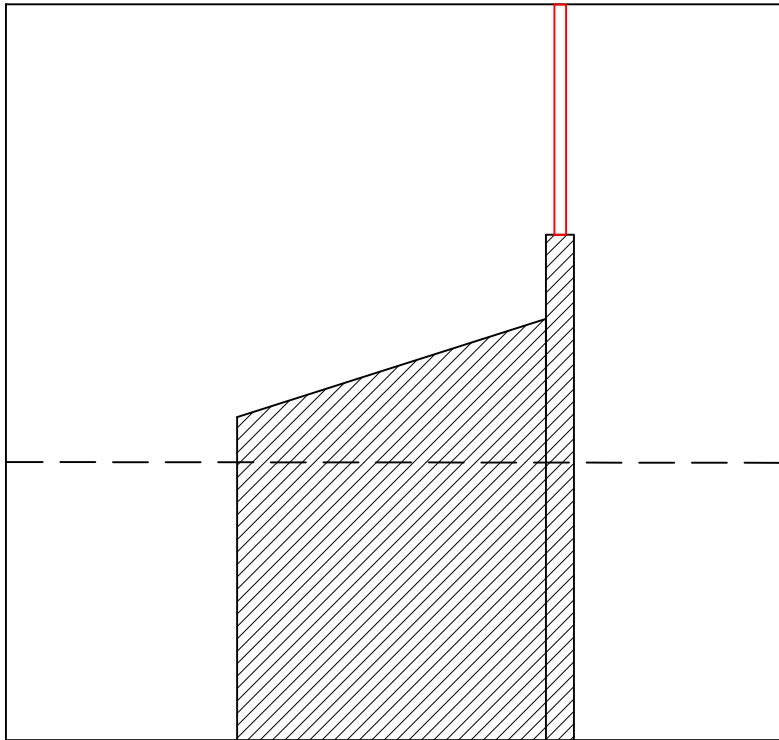
Figure 3.1: Flux surface for discharge

Chapter 4

Verification

Based on the above discussion, this thesis uses REEF3D::SFLOW to set up numerical water tanks, and tries to verify the reliability of the model through some primary calculation cases. The process of establishing numerical water tanks in REEF3D::SFLOW is divided into two parts. One is to create a water tank based on geometry and grid size. Related information is recorded in the control.txt file. The second is to set initial conditions, boundary conditions, wave parameters, etc. Related information is recorded in the ctrl.txt file. The process of verification is shown in the Figure 4.1.

The first case is a simulation of a regular wave propagating in an empty rectangular wave. The second case is a simulation of a regular wave propagating in a rectangular water flume with wedge object. The third case is a simulation of wave breaking in a rectangular water flume with a slope. After the study, simple wave behaviours in each case, a comprehensive forth case is considered involving multiple wave behaviours. It simulates wave propagation in a sizeable numerical domain with topography describing the real coastal environment in Mahamn harbour. This real scene verifies the feasibility of REEF3D::SFLOW in practical uses. During the verifications, wave deformations such as wave refraction, wave diffraction, wave diffraction, and wave breaking will be manifested.

4.1 Regular wave in rectangular tank with no obstacles

In the first case, the numerical water tank is rectangular, and there is no object in the water tank. Therefore, this example can be regarded as a one-dimensional water tank. The water flume has dimensions of 28m length and 1.0m height. The water
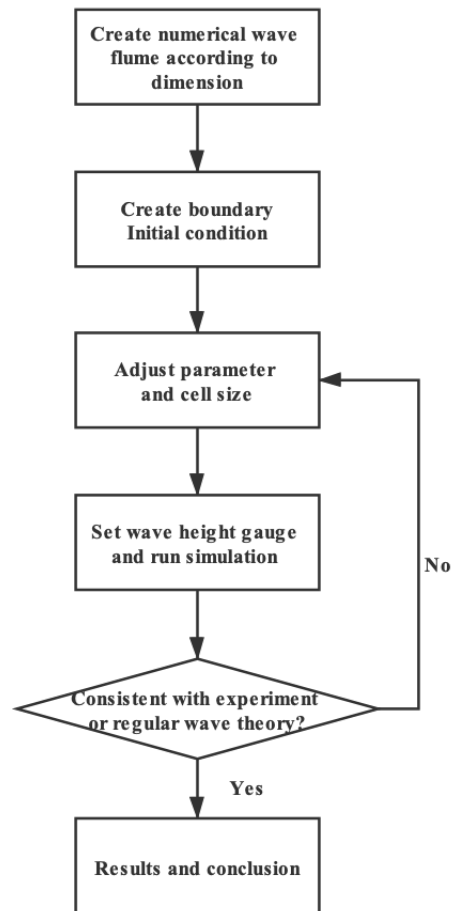
Figure 4.1: Verification process flowchart
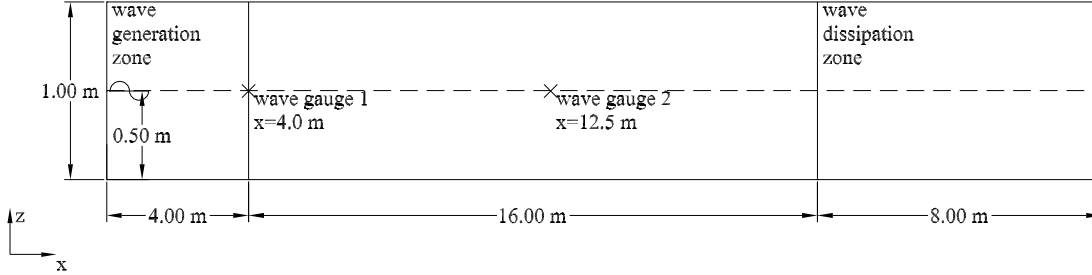
Figure 4.2: Case 1: Boundary setup for numerical water tank

level is constant at 0.5m the whole domain. Wave generation zone of 4m is at the beginning of flume and wave dissipation zone of 8m is at the end of the flume. Figure 4.2 shows the numerical wave flume dimension.

A regular wave with a wave height of 0.02m, a wavelength of 4.0m is simulated for 90 seconds. It is a low steep wave with the steepness of 0.005. The wave theory for generation wave is chosen to be the intermediate-depth wave theory. In addition, according to Wang's study, the CFL value 0.2 is a satisfactory parameter and will be applied to the following cases, unless further specified. With this condition, the wave profile from a successfully presented numerical simulation is supposed to match with the theoretical wave profile. A cell convergency study is presented with a cell size of 0.01m, 0.02m, 0.04 and 0.08m to define most rational simulation cell size. The wave profiles are obtained at t=90 seconds because at the moment the system is stable. Figure 4.3 shows the spatial fragment from x=6m to x=10m. The wave crests and the wave troughs in the domain are main focus. This region is also outside the wave generation region and the wave absorption region, which is completely used for calculation.. As can be seen, cell size of dx=0.01 has a cognizable difference in wave height and phase. Results of cell size dx=0.02, dx=0.04 and dx=0.08 have similar wave profile as the theoretical result, but dx=0.02 fits the theoretical curve the best. This phenomenon can be summarized as follow. For REEF3D::SFLOW, the numerical result improves precision on finer cells only in a proper convergence range, and dx=0.01 is out of range in this case. Therefore, in REEF3D::SFLOW, it is necessary to select the most appropriate cell size in the preliminary work to obtain more accurate simulation results. In this case, cell size of 0.02 is selected, and the number of cell units in the whole numerical flume is 70000. In the Figure 4.4,the results of the numerical simulation of the wave surface show that the measured wave profile near the wave generation boundary accords with the theoretical value to a high degree. With the increase of distance, the wave deforms to a certain extent,

23

which can be considered as energy dissipation. Therefore, the obtained wave profile will deviate from the theoretical solution as the wave propagates. As can be seen, the numerical result has slightly higher crests and higher troughs in the working zone from x=4m to x=20m. Overall it shows a good representation of wave propagation in reality.
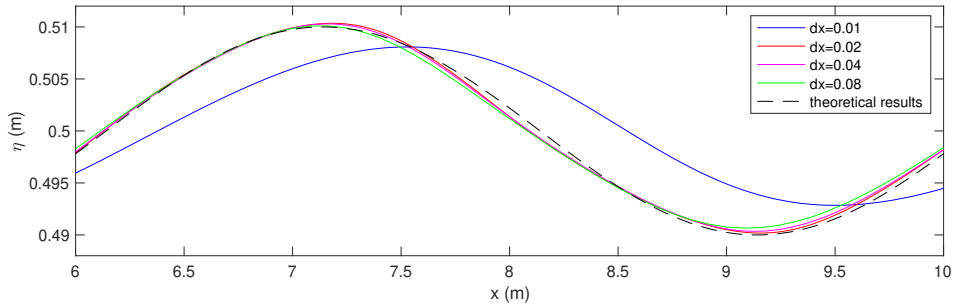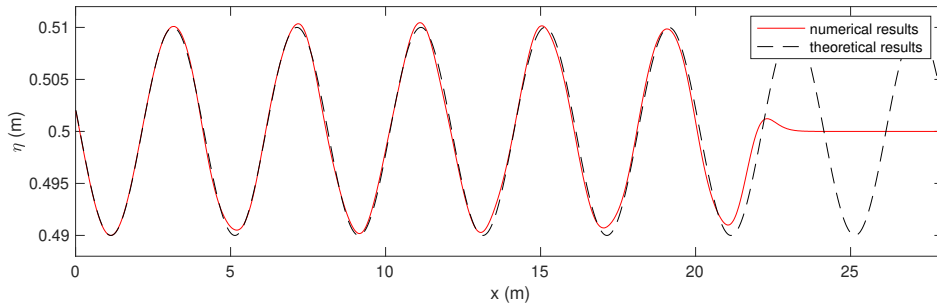

Figure 4.3: Case 1: Grid convergence study

Figure 4.4: Case 1: Comparison of free surface profiles at t=90s

Two height gauges WG1 and WG2 locate at x=4.0m and x=12.5m. Due to the location, WG1 directly monitors the wave profile outside of wave generation zone. WG2 locates in the middle part of water flume. The wave profiles in period from t=70s to t=90s are compared. At this period, the wave generator has been working long enough to stabilize the system to be studied. According to the calculation, the average wave height of WG1 is 0.02m, and average wave height of WG2 is 0.0195m. However, this small difference in wave heights is difficult to discern in Figure 4.5. As can be seen, the crest of WG1 is slightly higher than the WG2. Overall the wave profiles at two wave height gauges fit the theoretical values.

Paraview post-processes the numerical result. Visual figures of wave propagation are shown in Figure 4.6

24
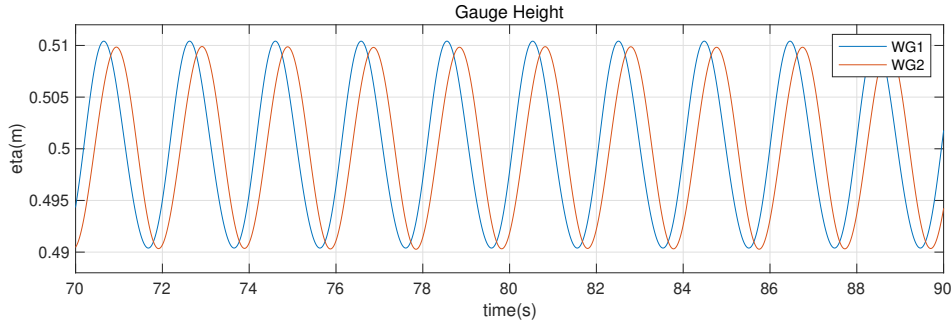
Figure 4.5: Case 1: Comparison of wave gauges
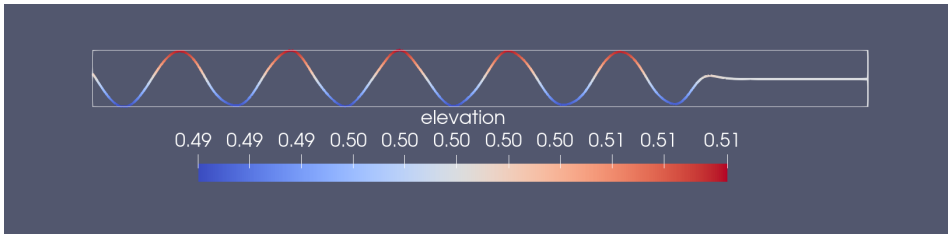
Figure 4.6: Case 1: Paraview post-processing surface image

4.2 Regular wave in rectangular tank with wedge object

In the second case, the dimension of the numerical rectangular tank is replicated as previous case. A wedge object with a steepness of 3:100 is placed in y-direction on the bottom of the flume. In this way, bathymetry contour is perpendicular to wavefronts. With water depth linearly increasing along y-direction, wave profile is expected to decrease as a wave propagating due to wave refraction. This case is considered to be a 2D numerical flume. Figure 4.7 shows the numerical wave flume setup.

In this case, the generation wave is the same as the generation wave in the first case. A regular wave with a wave height of 0.02m and a wavelength of 4m is simulated for 90 seconds. The wave theory is also based on the intermediate-depth linear wave theory.

Grid sizes of 0.02, 0.05, 0.08 and 0.10 are computed for cell size convergency study in Figure4.8 . As can be seen, all numerical results are off from theoretical results. This result is because of refraction. As the wave propagates along with the distance, wave height decreases. Also, wave profile dx=0.02 has a cognizable difference in wave height from other numerical results, so this cell size is not considered. Results of dx=0.05, dx=0.08 and dx=0.10 have similar wave profile as a theoretical result. The
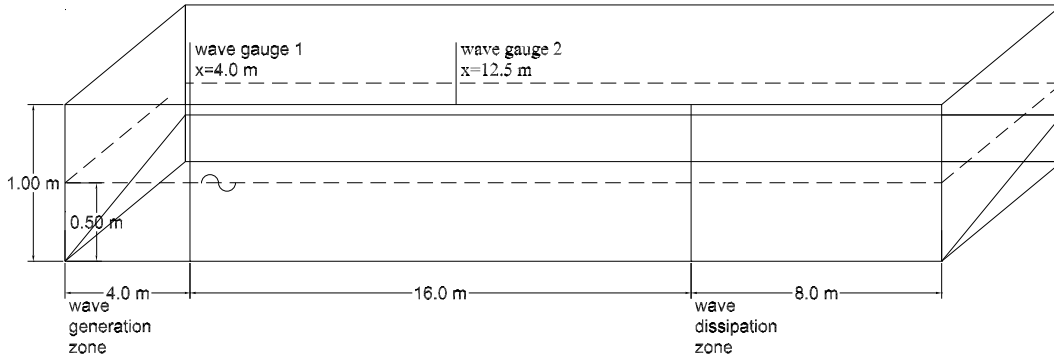
Figure 4.7: Case 2: Boundary setup for numerical water tank

grid cell of 0.05 is selected for better precision in this case. The number of cell units in the whole numerical tank is 2,240,000. In the Figure4.9 , the numerical result shows a decreasing pattern in wave crests and troughs in the working zone from x=4m to x=20m at y=0.1m, and this trend meets expectation because wave deformation of refraction phenomenon.
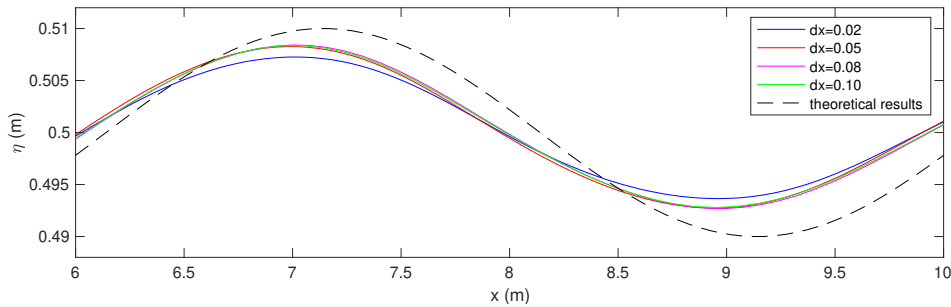

Figure 4.8: Case 2: Grid convergence study

Figure4.10 shows the water surface changes recorded by two wave gauges. It can be seen that the wave height at WG2 is significantly smaller than that at WG1 because it is far away from the wave generation boundary. However, Figure4.10 cannot directly indicate whether the phenomenon of refraction exists on the surface.
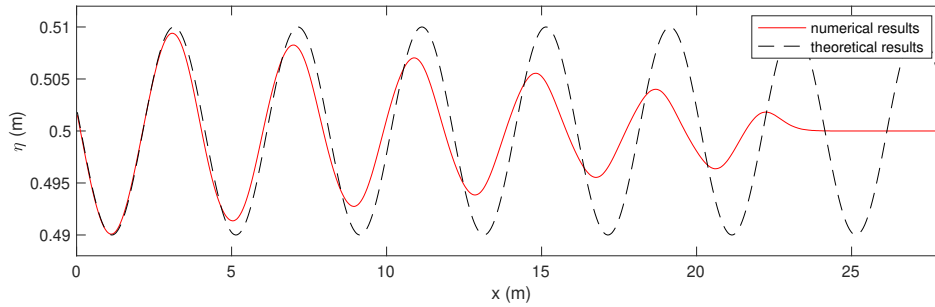
Figure 4.9: Case 2: Comparison of free surface profiles at t=90s
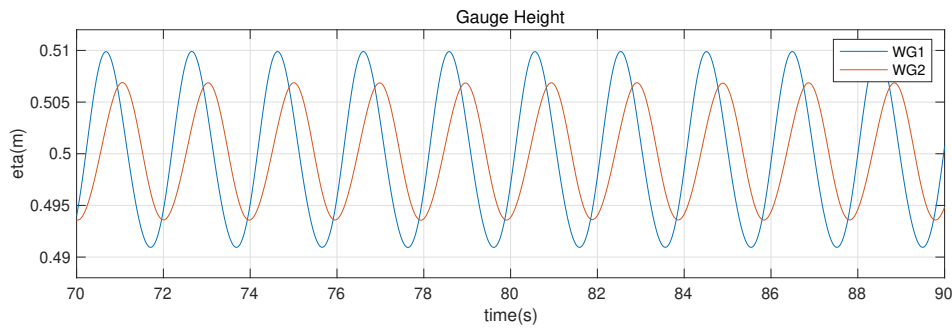
Figure 4.10: Case 2: Comparison of wave gauges at y=0.1m

The post-processing data of Paraview can be used to intuitively determine the refraction deformation phenomenon caused by the gradient in the y-direction. As can be seen in Figure4.11, wavefronts bend towards the shallow water area as it propagates towards the dissipation zone. Some waves in more bottomless zone catch up with the front waves in the shallow water due to higher velocity. Therefore wave orthogonal break, and higher waveheight occurs near the closed boundary before dissipation zone.
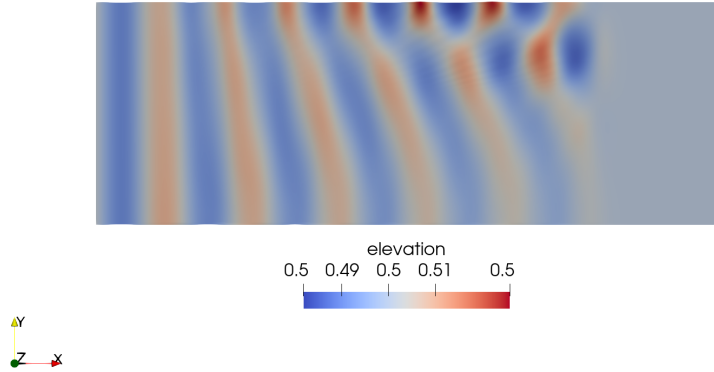
Figure 4.11: Case 2: Paraview post-processing surface image

In order to verify the accuracy of the model, the same generation wave is calculated in REEF3D::CFD method. The REEF3D::CFD result is compared with REEF3D::SFLOW as a reference. In order to compare the propagation and deformation of waves in both x-direction and y-direction, four data are selected. Figure4.12 shows the water elevation at x=4m and y=0.1m. Figure4.13shows the water elevation at x=12.5m and y=0.1m. Figure4.14 shows the water elevation at x=4m, y=9.9m. Figure4.15 shows the water elevation at x=12.5m y=9.9m. As can be seen, the results of REEF3D::SFLOW at each location are consistent with the results of REEF3D::CFD. Combined with the post-processed water surface visual map in Figure, it can be concluded with certainty that REEF3D::SFLOW has good simulation accuracy for wave refraction.
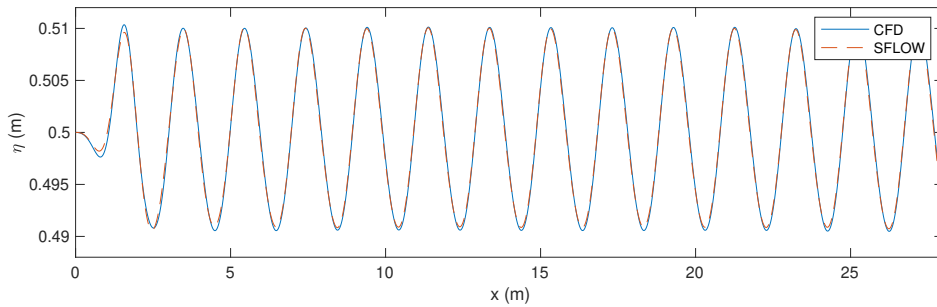
Figure 4.12: Case 2: Comparison of wave gauges at x=4.0m y=0.1m
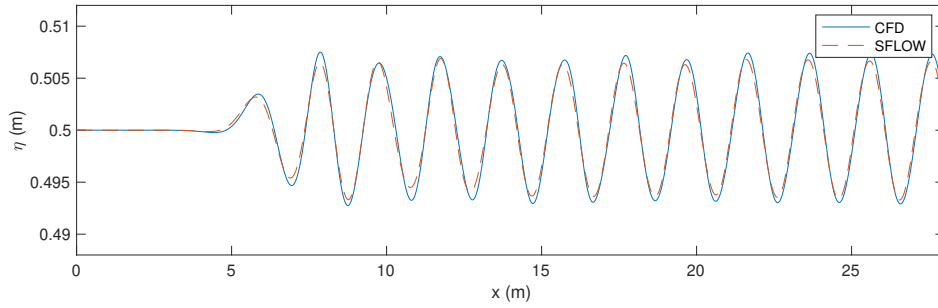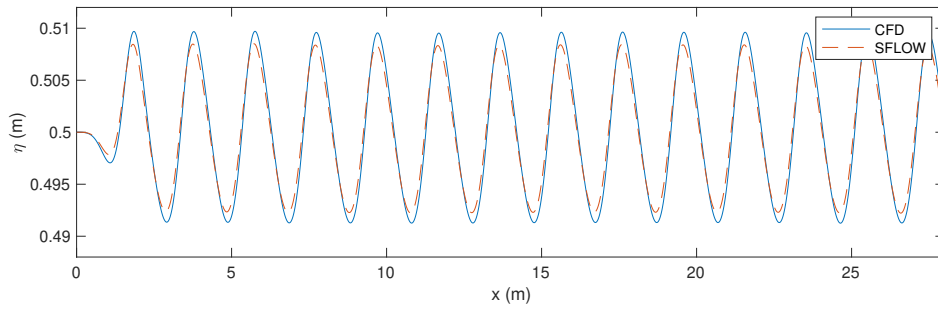
Figure 4.13: Case 2: Comparison of wave gauges at x=12.5m y=0.1m

Figure 4.14: Case 2: Comparison of wave gauges at x=4.0m y=9.9m

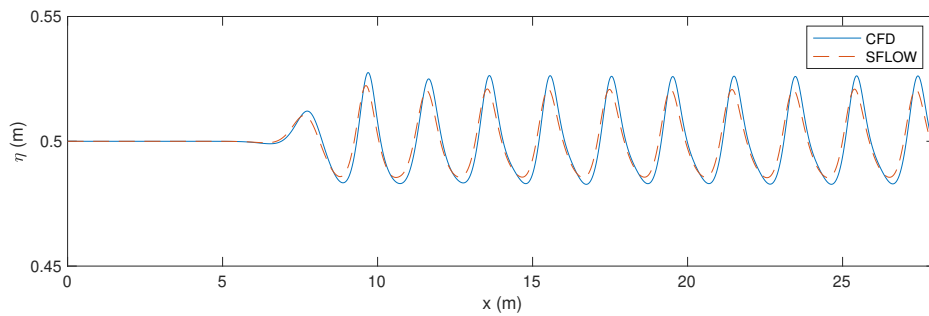

Figure 4.15: Case 2: Comparison of wave gauges at x=12.5.0m y=9.9m

4.3 Breaking wave in rectangular tank over a slope

This case is the verification of wave breaking accuracy. Breaking is one of the forms of wave deformation and influenced by wave steepness and bottom slope. Surging breaker, collapsing breaker, plunging breaker and spilling breaker are the common breaker types to be observed.

The water flume has a length of 40 m and a height of 1m. The original water level is 0.4m for the numerical domain. A slope with the steepness of 1:35 is placed at a distance of 13.8m away from the inlet to the end. The slope has a height of 0.748m at the end of the flume. Wave generation zone and wave dissipation zone have a length of 9.81m, located on each side of the flume. As shown in the Figure4.16, water depth will gradually decrease as the waves propagate.
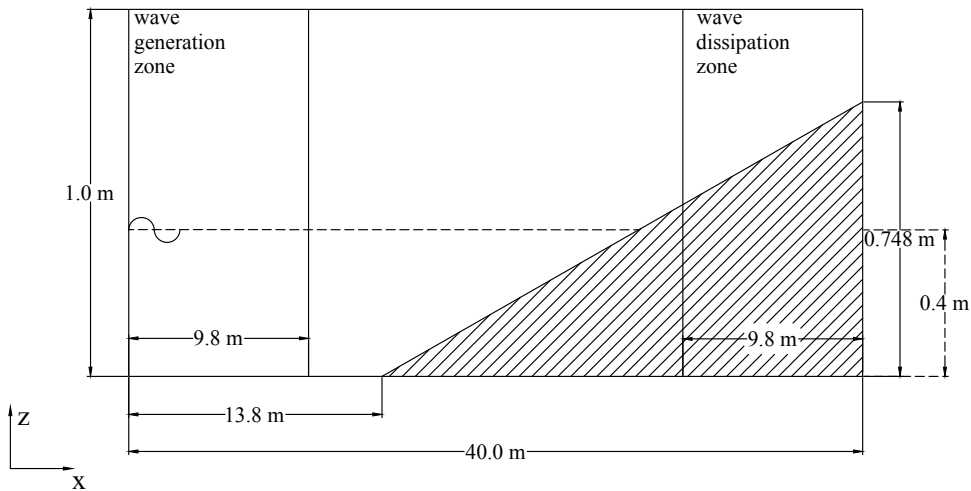

Figure 4.16: Case 3: Boundary setup for numerical water tank

A fifth-order Cnoidal wave with a wave height of 0.128m, wave period of 5.0s is simulated for 40 seconds. The steepness is calculated to be 0.057. With Iribarren number of 0.5, plunging breaker is expected. Because this case is about verifying wave breaking. When determining the size of the grid, the wave profile close to breaking on the slope is the most critical. Figure4.17 shows the study on the convergence of the wave grid at wave gauge 4. In Figure4.18 the difference between the data is more obvious. As shown in the figure, the larger the grid size, the more the wave profile deviates from the experimental value. On the premise of ensuring computational efficiency, dx=0.005m is the most suitable grid size.The cell size of 0.005m is selected in this case, and the number of cell units in the whole numerical flume is 304 000.
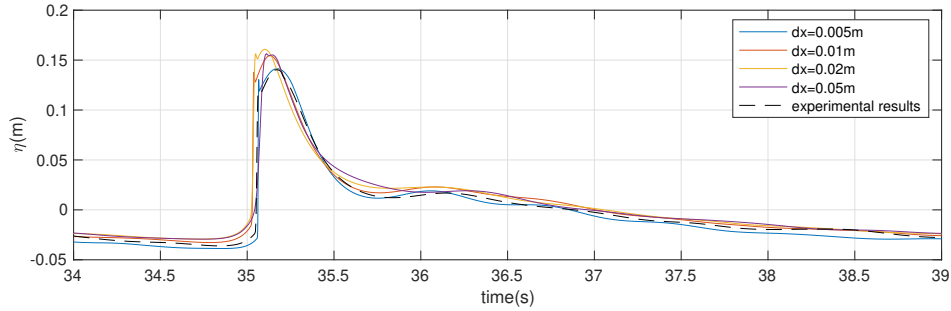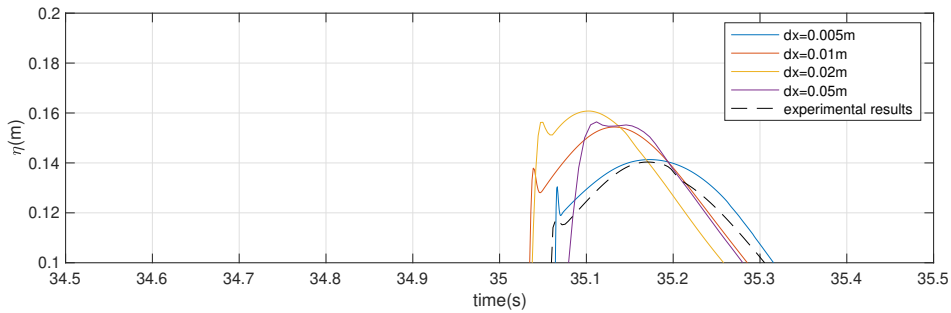
Figure 4.17: Case 3: Grid convergence study

Figure 4.18: Case 3: Grid convergence study

Four wave heights locate on the slope. By comparing second and third numerical wave crests after simulation starts, WG2 has higher wave crests than WG1. This situation is due to shoaling as wave climbs on the slope. First wave crest in time series is not depicted because the system needs time to be stable for valid and reliable data. Wave crests measured by WG3 and WG4 decrease gradually with recognizable tips in the front. These tips show the unstable crests occur at WG3 and WG4. These situations indicate breaking happens between WG2 and WG3, between x=20.8m to x=21.8m and wave dissipation continues at x=22.1m.
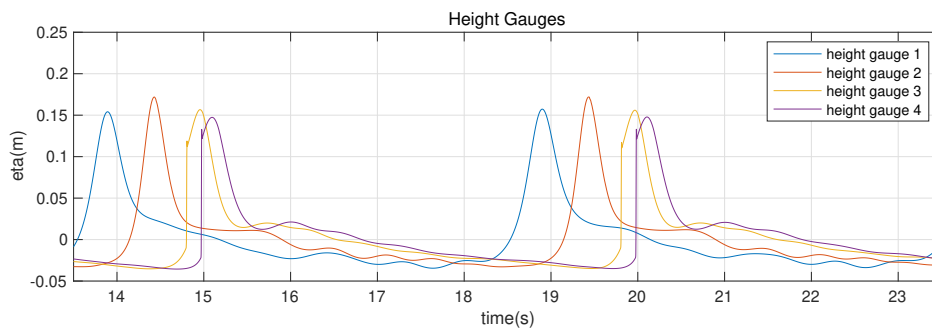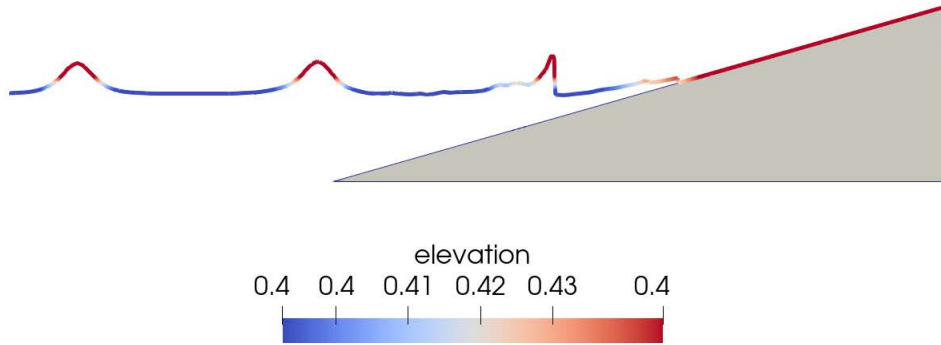

Figure 4.19: Case 3: Comparison of wave gauges

31

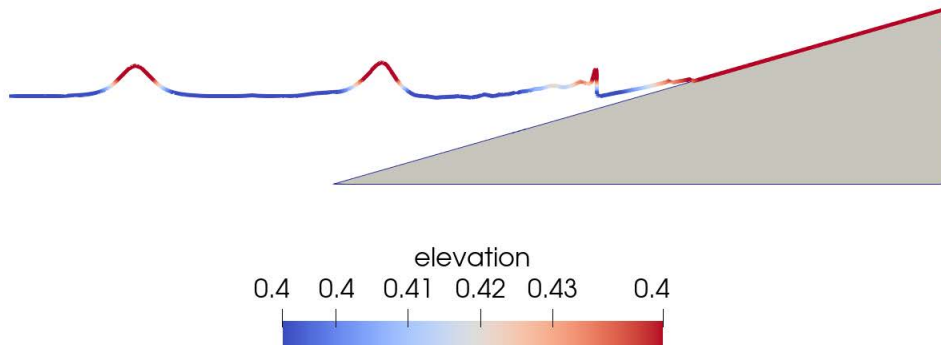Figure 4.20: Case 3: Paraview post-processing surface image at t=35.00s

Figure 4.21: Case 3: Paraview post-processing surface image at t=36.00s

Post-processing figures can virtually describe this phenomenon. As wave moving towards the slope, wave crest increases until a position where wavefront is vertical. As the post-processing figures shown, it is the position where the break happens. After breaking starts, wave height decreases as it approaching further on the slope until energy entirely dissipates. Meanwhile, the next wave crest follows and increasing along the slope until it breaks.
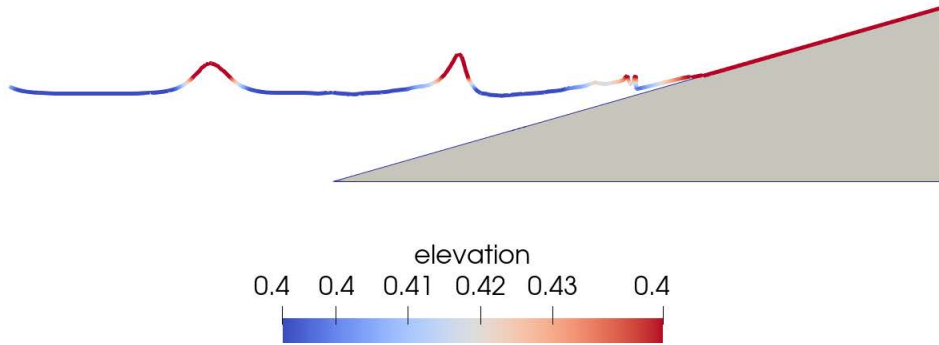
Figure 4.22: Case 3: Paraview post-processing surface image at t=37.00s

The post-processing figure can intuitively prove the process of wave breaking. However, the accuracy of the numerical model simulating wave breaking needs to verify with experimental data. As shown in the figures comparing the simulation results with theoretical results, in the time period from t=15s to t=20s, the wave profile is most suitable for the experimental data. At most wave crests, the numerical simulation results are slightly higher than the experimental results. Over time, the difference between the wave and the experimental result is more natural to observe at the trough. At the position of the third wave gauge where x=21.8m, there are small tips on the wave profile shown. This pattern can formally prove wave deformation process.
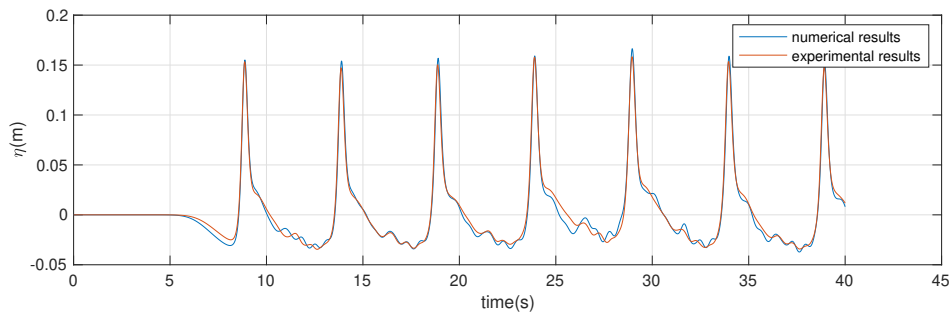
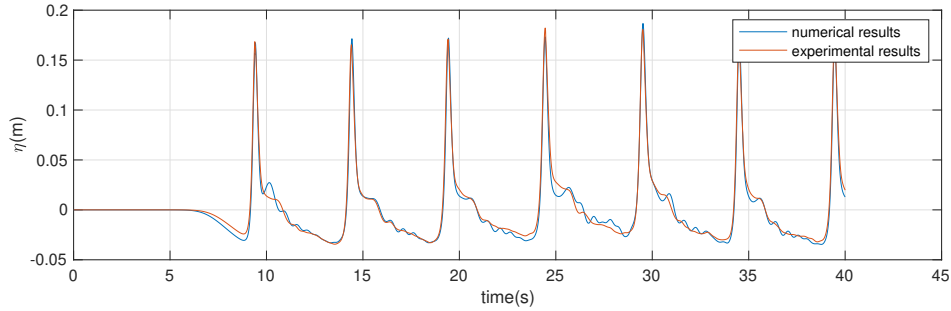

Figure 4.23: Case 3: Comparison of wave gauges at x=19.8m
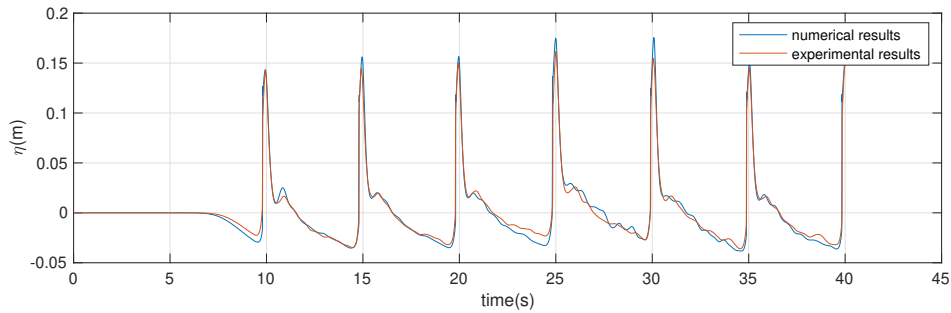
Figure 4.24: Case 3: Comparison of wave gauges at x=20.8m

Figure 4.25: Case 3: Comparison of wave gauges at x=21.8m
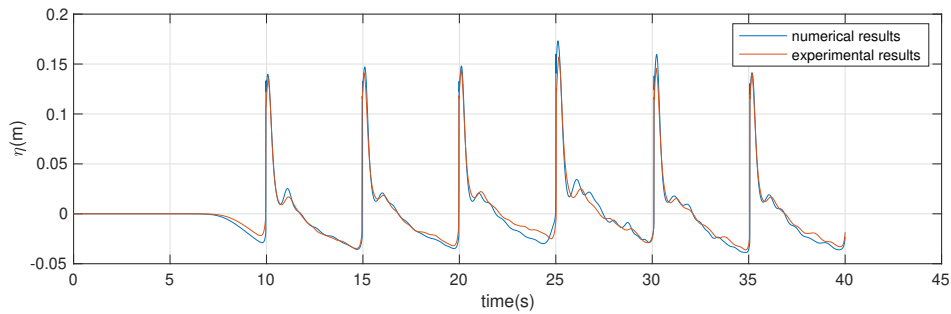
Figure 4.26: Case 3: Comparison of wave gauges at x=22.1m

4.4 Large-scale simulation of wave propagation at Mehamn harbor

In the third case, wave propagation in Mehamn harbor is simulated to verify the accuracy of REEF3D for large-scale simulation. Mehamn locates on Vedvik peninsula shown as red spot in the Figure4.27. It is a north port of Hurtigruten's classic route in Norway. Eastern and western land protects Mehamn harbor as natural barriers. On the north side, the Mehamn harbor is open to Barrent Sea and affected by swell. The topography is relatively moderate, and the water depth is treated as an intermediate

34

Figure 4.27: Case 4: Mehamn harbor location

water depth condition in this case.

Map is zoomed in and rotated for convenience in numerical simulation computation, shown in Figure4.28. A rectangular water flume has a length of 1760m in the southwest direction, a width of 1440m in southeast direction and height of 105m. The water level is 57m over the domain. Wave generation zone of 360m is located at the beginning of water flume to simulate wave from the open sea. Adjustment of wave dissipation zone of 360m is considered regarding Mehamn harbor location. The numerical wave tank is shown in Figure4.29.

The generated wave is a Second-order Stoke wave with a wave height of 3.5 meters, wave period of 9.5 seconds and a wave phase of 0. In this case, there are 16 height gauge measuring water level shown in the figure. The cell size of 5m is selected in this case, and the number of cell units in the whole numerical flume is 2128896.
The figure shows the surface elevation of the numerical domain at simulation time t=600s. Stable refraction is noticeable along the northeast(left) side of the more prominent peninsula and some weak refraction locates along the northeast side of smaller peninsula inside the harbor. As wave propagating into the harbor, wavefront bends around and penetrate the lee side of the peninsula, which can be inferred as a diffraction pattern. As the wave propagates inside the harbor, wave height reduces as topography rises moderately and result in a visible shoaling pattern.
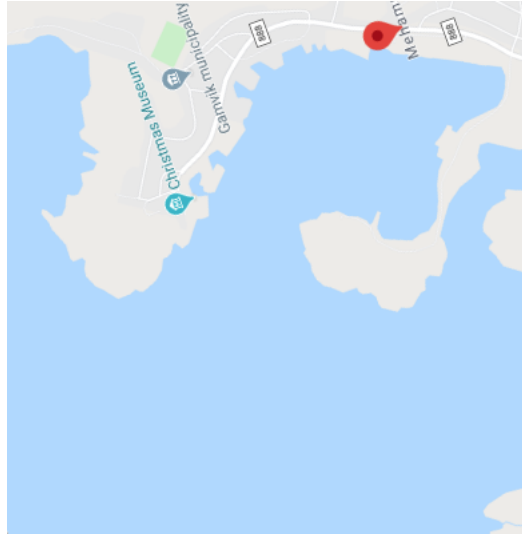
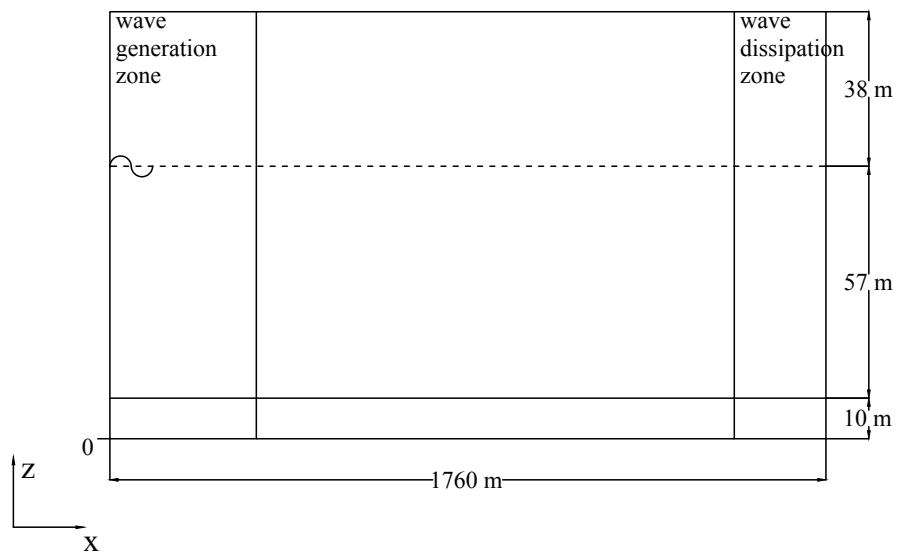Figure 4.28: Case 4: Mehamn harbor location

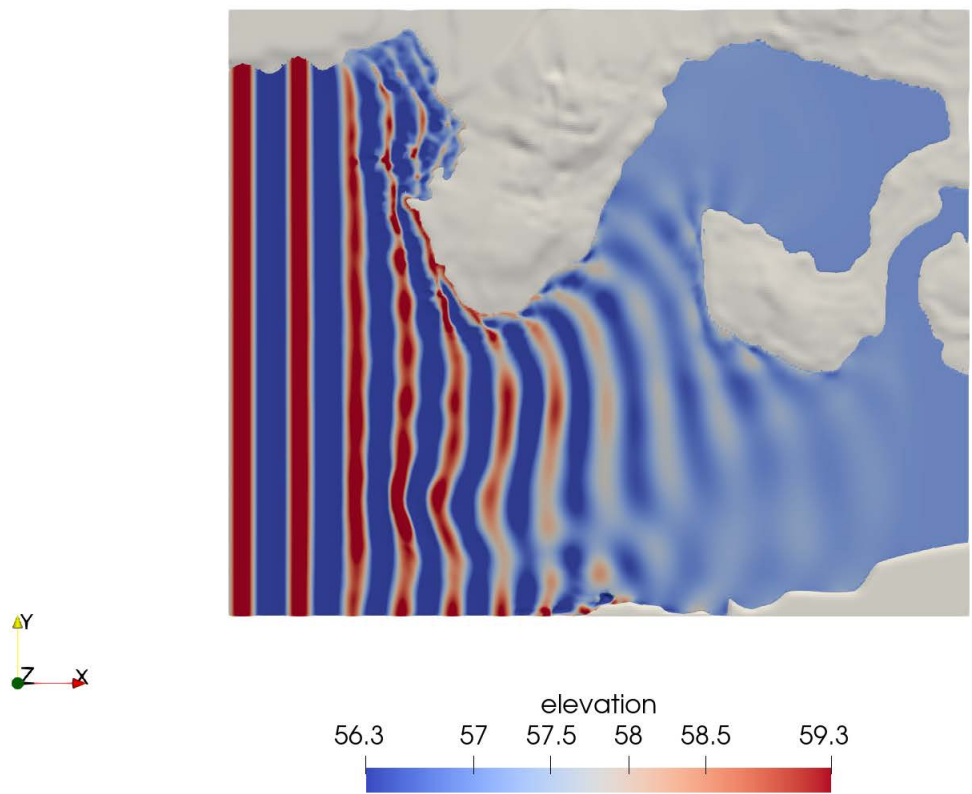Figure 4.29: Case 4: Boundary setup for numerical water tank

Figure 4.30: Case 4: Wave propagation in Mehamn harbor

Chapter 5

Investigation on Wave Overtopping

In the previous section, regular wave scenarios, breaking wave scenarios and large scale wave propagation over real topography are simulated to verify REEF3D::SFLOW feasibility. REEF3D::SFLOW can effectively simulate various characteristics of wave propagation near shore, and the computed results can be used in scientific research and engineering projects. Nowadays, coastal projects are often complex in structure and many known semi-empirical formulas cannot be applied to complex structures. The main focus of this chapter is the application of REEF3D::SFLOW as a tool to investigate wave propagation on intricate structures, especially wave elevation and wave overtopping.

A case of simulating regular wave propagation on a complex coastal structure is studied in this chapter. The studied model is referred from A. Mokos published case report in 2020 about simulating wave overtopping on a complex coastal structure using SPH[30]. In this chapter, a summary of the complex coastal structure elements is given, followed by the detailed simulation domain setting up process. The simulation data is compared with experimental measurement to determine model validation. The measurements of the physical experiment are based on the figures of A. Mokos report. Matlab GUI subroutine named Image2Data[44] is used to obtain accurate physical experiment data from Mokos' report[30]. The free surface position at designed wave gauges and the overtopping volume are studied. Finally, this chapter simulates the effect of sea level rise on the overtopping discharge under different representative concentration pathway scenarios.

5.1 Experimental setup

In this chapter, a complex double-dike defence structure is studied for the effect of sea level rise on wave overtopping. Figure5.1 shows an overall sketch of a physical

experimental setup in Mokos's report. The physical wave tank has dimensions of 60m in length, 1.5m in width and 1.2m in height. The static water depth inside wave tank is 0.66m. The first part of the water wave tank simulates a water channel of 52m in length. A slope with the steepness of 0.05 is placed at location 17.5m away from the beginning of the channel. The slope levels up the channel bottom to 0.2m at location 21.5m away from beginning and the channel bottom stays constant until it reaches the dike structure. The second part of the wave tank is defence structure consists of two dike elements. The details about two dike elements are shown in Figure5.2. The first dike element is rectangular with 0.52m in length and 0.59m in height. The first dike is supposed to be submerged in order to simulate potential flooding condition. The second dike element has a quadrangle shape with a slope on the top. The slope steepness is 0.015 and increases second dike height from 0.48m to 0.62m. The second dike is supposed to be submerged as well during the experiment. A wall with a width of 0.04m and height of 0.74m is placed right behind the second dike, followed by a water gathering tank to measure the overtopping volume of the structure. The emersed wall stops water from running into the water tank before the wave generator starts. The generated wave has a wave period of 2s and a wave height of 0.22m. The wavelength calculated by wave dispersion relation is 3.941m. A. Mokos calculates the wave celerity for shallow water wave is 2.54m/s[30].
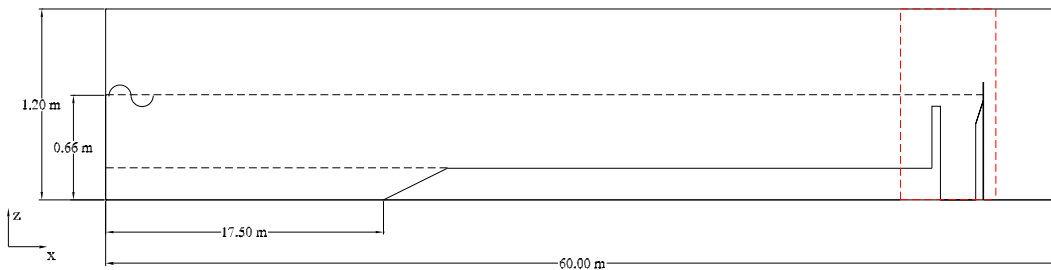

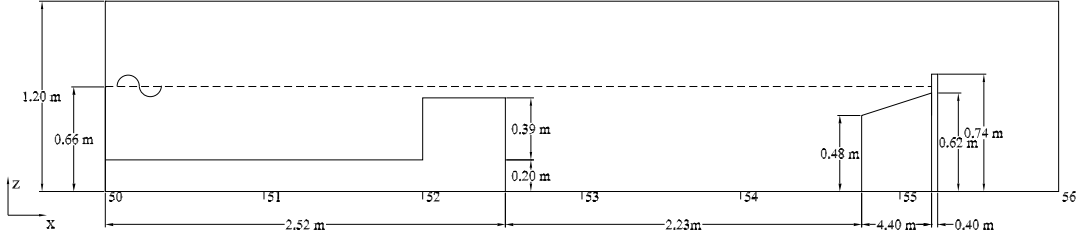Figure 5.1: Dike structure overall design

Figure 5.2: Dike structure element design

Table 5.1: Position of different elements of structure in physical experiment

Elements	Position (m)	Height (m)
Wave generator	0.00	0.00
Slope start	17.50	0.20
Slope end	21.50	0.20
First dike start	52.00	0.59
First dike end	52.52	0.59
Second dike start	54.76	0.48
Plateau start	55.20	0.62
Final wall	55.24	0.74

Table 5.2: Position of wave gauges

WG	1	2	3	4	5	6	7	8
x(m)	15.00	30.01	30.02	30.42	30.67	31.65	42.00	46.00
WG	9	10	11	12	13	14	15	
x(m)	50.00	51.50	53.00	53.50	54.00	54.50	55.00	

5.2 Simulation setup

The two-dimensional numerical wave tank is 16m long, 1.5m wide and 1.2m high. For computation efficiency, the channel length of the physical experiment is shortened. The wave generates at a distance of two wavelengths (8m) away from the first dike element. This distance enables the wave maker to generate stable waves before waves reach the operation zone where dike elements locate. The slope that levels up channel bottom by 0.2m in the physical experiment is ignored in the numerical simulation. The channel bottom is at 0.2m from the beginning of the numerical wave tank to simulate the last 8m of the physical water channel. Therefore all structural elements

40

are relocated to new positions in the simulation. The specific values of each element are shown in the Table5.3. The wave gauges locations are shown in the Table5.4

Table 5.3: Position of different elements of structure in numerical simulation

Elements	Position (m)	Height (m)
Wave generator	0.00	0.00
Levelled bot start	0.00	0.20
Levelled bot end	8.00	0.20
First dike start	8.00	0.59
First dike end	8.52	0.59
Second dike start	10.76	0.48
Plateau start	11.20	0.62
Final wall	11.24	0.74

Table 5.4: Position of wave gauges in numerical simulation

WG	1	2	3	4	5	6	7	8
x(m)	NA	NA	NA	NA	NA	NA	NA	2.00
WG	9	10	11	12	13	14	15	
x(m)	6.00	7.50	9.00	9.50	10.00	10.50	11.00	

The second-order Stokes wave theory is applied as the wave generation method. The designed wave height is 0.22m, and the wave period is 2s. At initial condition, the water depth is 0.66m over the whole wave tank domain. In order to limit effects by secondary reflection and transmitted waves from structure elements, wave generation and absorption method are set as the relaxation method. A wave generation zone of 4m is set at the inlet of wave tank, and a wave dissipation zone of 4m is set at the outlet of the wave tank. The main structural elements for dike system are located in the operation zone of numerical wave tank from 4m to 12m. The Courant-Friedrichs-Lewy number in this model is 0.3, set as same as applied in A. Mokos physical experiment[30]. The total simulation time is 40 seconds. The first 15 seconds allows the wave propagates to the dike structure. Within the next 5 seconds, the waves propagate over the complex structure and deform for the first time. In the remaining time, the system is gradually stable for data record and analysis.
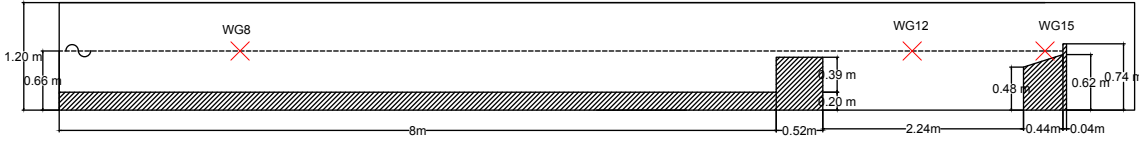
Figure 5.3: Dike structure in simulation

There is a summary of the differences between the physical experiment setup and the numerical wave tank setup:

1. In the numerical simulation, regards to simulate efficiency, water channel is shortened to 8m. According to Mokos' calculations, the designed wavelength is 3.941m[30]. Therefore, the number of waves on the ignored wave channel (44m) is non-integer. This indicates there is a time difference when waves arrive at the water gauge location. The figures about Mokos experiment measurements in this chapter are all slightly adjusted in the timeline to compare with the simulation results.

2. The channel slope design is cancelled in the simulation. Therefore, the measurement of wave elevation along the water channel may experience nonlinear due to channel slope in the physical experiment.

2. In Mokos physics experiment[30], waves are generated by piston wavemaker. In the numerical wave tank simulation, the second-order Stokes wave theory is applied as generate wave theory.

3. At the initial position of Mokos' physics experiment[30], the overtopping collect tank behind wall element is empty. In contrast, in the numerical simulation, the initial water depth is 0.66m over the whole wave thank domain, including the domain behind the wall element.

5.3   Analysis of wave elevation

In order to verify whether the numerical water tank established by the above method is valid, the simulation results and experimental data are compared. The difference is observed to verify whether the degree of fitness meets the requirements. However, before comparison, the convergence of the cell needs further verification.

The wave profile recorded by WG8 is selected because the wave is still stable before it interacts with the first dike element, as shown in Figure5.3. The time period is selected to be 38s to 39s because operation time is long enough to generate a stable wave profile. According to Figure 5.4, simulation of cell size 0.1, 0.15, 0.2 and 0.3 are compared with the experiment measurements. As can be seen, the cell size of 0.1, 0.15 and 0.2 have similar patterns as the experimental measurements, therefore shows

the convergency. Wave profile of cell size 0.1 has little difference from the wave profile of cell size 0.15. But the wave profile of cell size 0.3 does not fit the experimental measurement sufficiently. Therefore, the cell size of 0.1 and the cell size of 0.2 are chosen in this model. By comparing the simulation results of two different cell sizes, the pattern of resolution on the simulation can also be analyzed in this section.
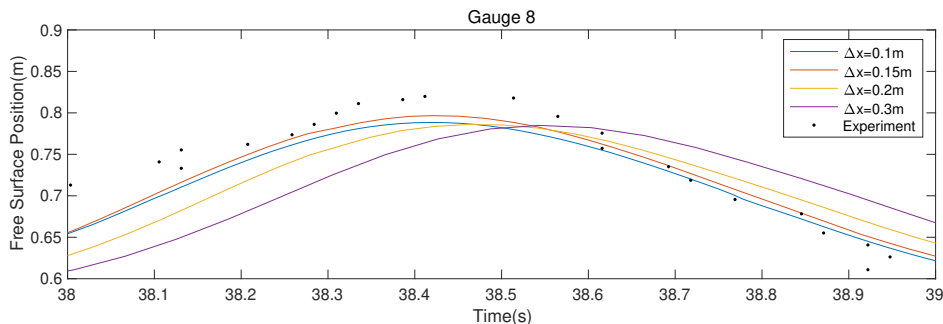

Figure 5.4: Cell convergence study of overtop simulation

Wave profiles at the three wave gauges WG8, WG12 and WG15 are compared with the experimental measurements from A. Mokos report[30].

The comparisons of simulation wave elevation and experiment measurements at location WG8 are shown in Figure5.5. The wave troughs of simulation results are higher than the experiment measurement. The trough differences have a range from 0.03m to 0.05m. In the period between t=20s to t=26s and the period between t=36s to 40s, the crests of simulation results are lower than the experimental measurements. The range of differences is between 0.02m to 0.03m. In the period between t=26s to 36s, the difference of crests position reaches the maximum of 0.08m. The experimental measurements also show relative small surface vibrations near the troughs, for example near t=32s, the sixth wave trough in the figure shows small decomposition, which is not recognisable in the simulations. Overall, the simulation overestimates the wave troughs and underestimates the wave crests. These differences between the simulation and the experiment can be explained by two reasons. First, numerical simulation ignores the slope of the channel bottom. In the physical experiment, the slope levels up the channel bottom to 0.2m at a distance of 17.5m from the inlet of a wave tank. The decrease of water depth in the physical experiment causes wave shoaling and wave height increases as the wave propagates over the channel slope. Second, the waves in the physical experiment experience the reflection waves from the wall element. These reflected waves travel in the opposite direction and increase the wave elevation at the location of WG8. In the numerical simulation, the waves in wave generation zone are stable and are not influenced by any reflected waves or transmitted waves.
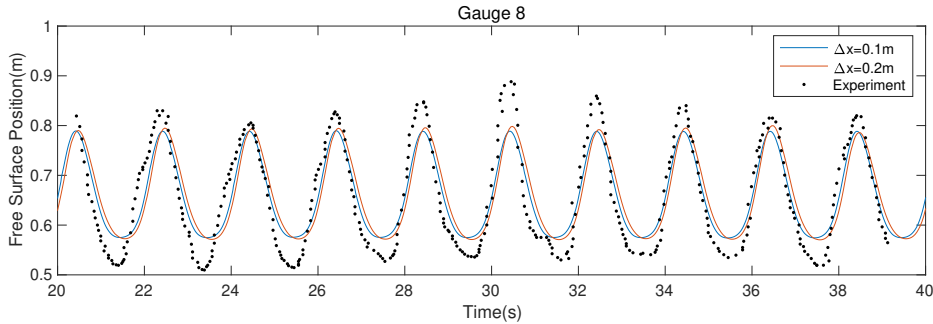
Figure 5.5: Comparison of free surface profiles at WG8

The comparisons of simulation wave elevation and experimental measurements at location WG10 is shown in Figure5.6. Overall, the simulations underestimate the wave crests but predict the nonlinearity of wave profile. Also, the difference between cell sizes is recognizable. The simulation result of finer cell size 0.1m shows similar wave profile shape as the experiment, especially in the last 15 seconds of the simulation. The wave decomposition between the two dikes elements is shown. However, the simulation result of cell size 0.2m is not able to predict the wave decomposition, although it predicts the wave troughs position accurately. The differences between the simulation and experimental measurements can be explained by the complex structures of the model. The waves propagate over the first dike element are influenced by the reflected wave from the second dike element in the physical experiment. Any small interaction difference between waves and structures result is amplified during the simulation. Besides, Figure5.6 shows that the cell size limits the resolution of wave surface information. Finer cell size in the cell convergence may improve the simulation results.
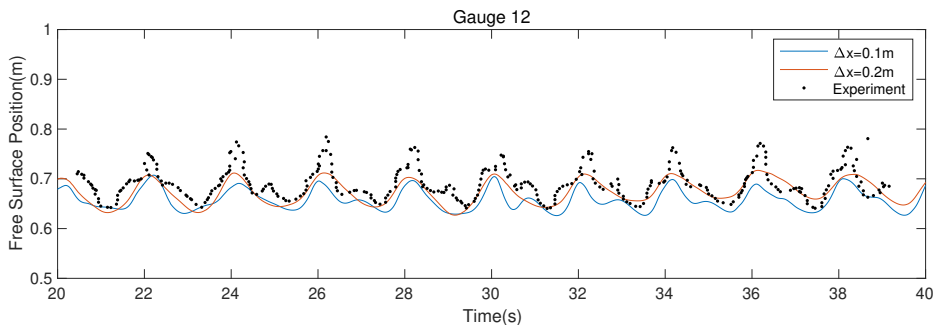

Figure 5.6: Comparison of free surface profiles at WG12

At location of WG15, the situation is similar to WG12. Wave profile of cell size 0.1m is much similar in shape with the experimental result. This phenomenon means that

result of cell size 0.1m simulation can predict decomposition of waves. Compared to the experiment, wave profile with a cell size of 0.2 has peak and trough positions similar to the experimental elevation. However, the wave profile with cell size of 0.2 has more apparent fluctuations. Result of cell size 0.2m overestimates the deformation of decomposed waves. Result of cell size 0.1m predicts the decomposition more accurate because the degree of fluctuation pattern near wave troughs fits the experimental measurement. However, the result of cell size 0.1m has lower wave trough prediction than the experimental measurement. The differences between crests and wave troughs increase with the simulation time. The most consistent simulation result to the practical wave propagation is the result of cell size 0.1m at the period between t=20s to t=25s. .
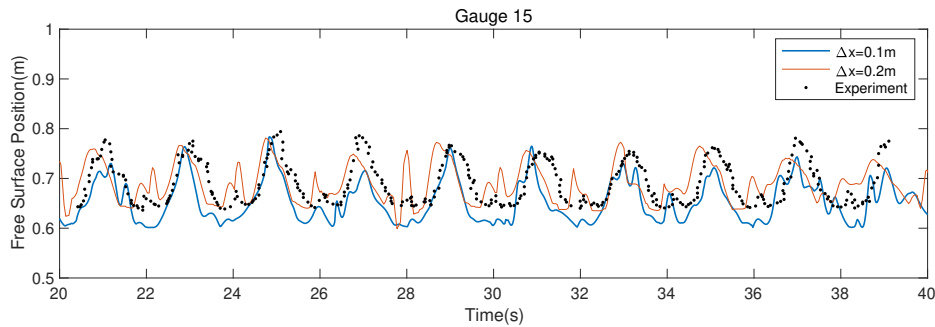

Figure 5.7: Comparison of free surface profiles at WG15

In summary, the numerical results at locations WG8, WG12 and WG15 differ from the experimental measurement considerably. Although the locations of wave troughs are not accurate for both cell size results, the wave profile of finer cell size 0.1m shows a similar fluctuation pattern. Result of cell size 0.1m simulation can predict the decomposition and wave nonlinearity of wave propagation more accurately. Because the above figures describe the wave propagation at specific wave gauge, THe wave elevation changes are compared in time series. Therefore, these figures cannot adequately describe the wave propagation over the whole defence structure.

Paraview post-processed images show the process of wave propagation directly and provide more details. In Figure5.8 to Figure5.12 the selected wave profiles between period t=22.5 to t=23.2 are shown by simulation data after post processed. The wave propagation over the whole structure can be analyzed in three parts. First, the stable regular wave travels towards the first dike element. As the wave travelling closer to the dike element, the nonlinearity of wave deformation appears. When the wave travels over the first dike element, wave decomposes into shorter waves. This phenomenon can be found in Figure5.8, Figure5.9 and Figure5.10. The transmitted

waves over the first dike element propagate as nonconservative waves and several higher frequency harmonics appear due to the energy transformation of the system. Second, the wave propagates from the first dike element towards the second dike element. The surface elevation is complex because the wave experiences the reflected waves from the coming obstacle wall and wave nonlinearity due to slope of second dike. Third, when wave propagates on the slope of the second dike element, wave deforms due to the shoaling effect. At the wall, wave crest reaches a considerable height and breaks. The overtopping wave falls under the force of gravity behind the wall. The remaining water blocked by the wall element results in reflected wave and propagates in the opposite direction. This portion of the wave will soon be cumulated with the next coming wave.
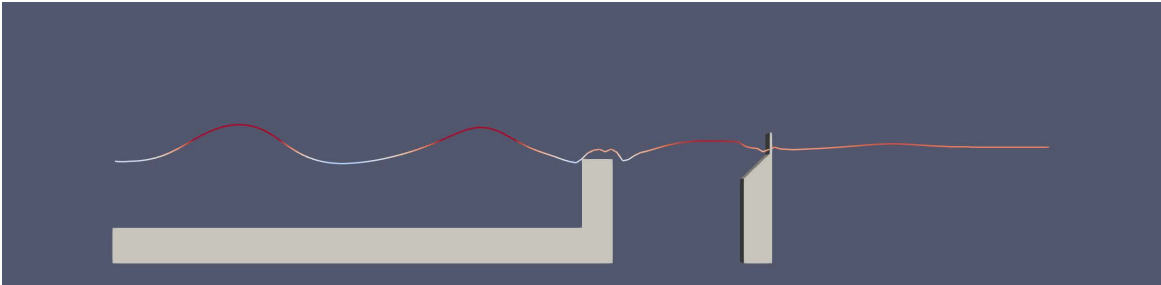

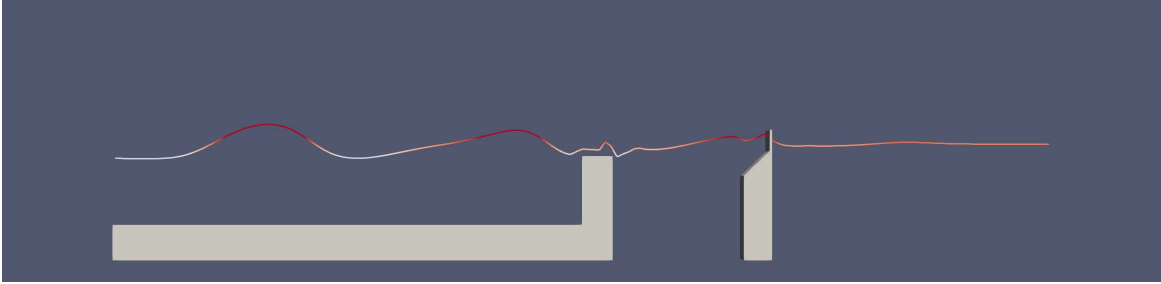Figure 5.8: Paraview post-processing surface image at t=22.5s

Figure 5.9: Paraview post-processing surface image at t=22.7s

5.4 Analysis of overtopping

Figure5.13 shows the exceed wave elevation over the wall crest at location x=11.2m between t=20s to t=40s. . As can be seen, on average, every 2 seconds, there is a wave with an elevation higher than the wall crest. For every wave overtopping, the exceed water elevation over the structure crest is different, which indicates that there is a certain randomness in the process of wave overtopping. The average maximum
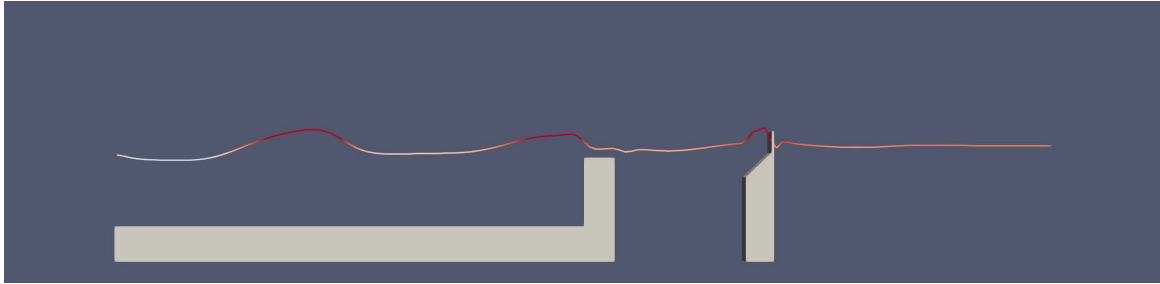
Figure 5.10: Paraview post-processing surface image at t=23.0s
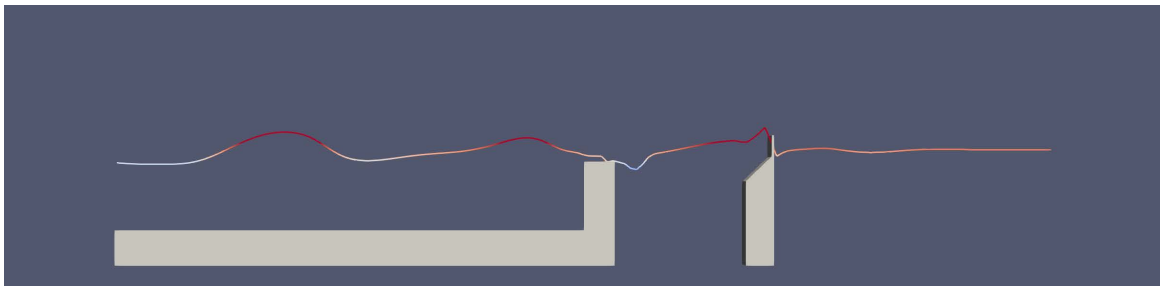

Figure 5.11: Paraview post-processing surface image at t=23.1s
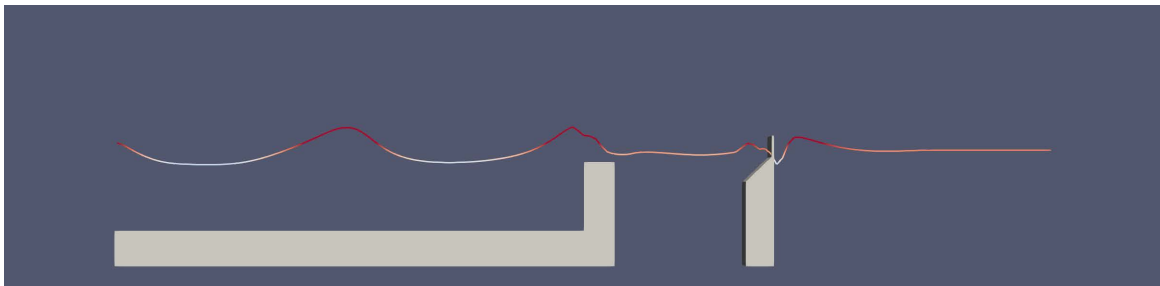

Figure 5.12: Paraview post-processing surface image at t=23.2s

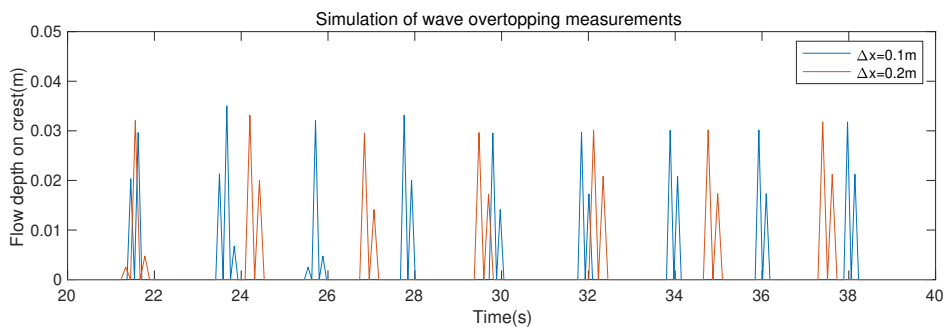of the excess water elevation is 0.03m higher than the structure crest.

Figure 5.13: Water depth over structure crest

The data in the physical experiment does not include the time change of overtopping, but only the final overtopping value and total time. Therefore, it is assumed that the overtopping volume in the physical experiment increases linearly. The Figure 5.14 shows the evolution of overtopping volume at two different resolutions. The simulation data result with a grid size of 0.2 is lower than the experiment. At a coarser resolution, the wave surface fluctuates greatly, so the simulation results should be quite different from the experimental results, which is also in line with expectations. As the resolution becomes more precise, the simulated data with a grid size of 0.1 is very close to the experimental data. At this resolution, for this dike design numerical simulation, the amount of surging is slightly higher than the experimental data. For engineering design, this is a safe simulation because the simulation is not underestimated and result is in line with expectations.
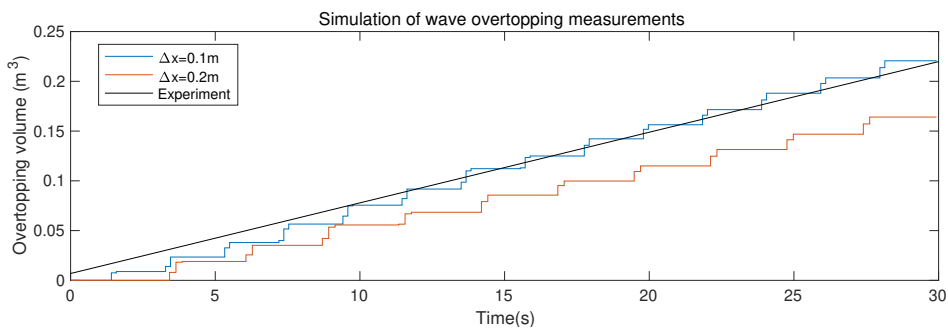

Figure 5.14: Overtopping volume comparison for REEF3D::SFLOW with the experimental results

In order to understand the impact of sea level rise on overtopping, in the existing numerical simulation tank model, the initial water surface is reset to the future sea level predicted by IPCC, as shown in the table:

Table 5.5: Projections of global mean sea level rise

Emission Scenario	Low	Medium	Medium	High
Representative Concentration Pathway (RCP)	2.6	4.5	6.0	8.5
2100 CO 2 concentration (ppm)	421	538	670	936
MSLR (m) 2046-2065	0.24	0.26	0.25	0.29
MSLR (m) 2100	0.44	0.53	0.55	0.74

In this section, a total of eight sets of overtopping evolution under different water surfaces are simulated. They are the sea level after sea level rise in 2065 and 2100 under the four emission scenarios of RCP2.6, RCP4.5, RCP6.0 and RCP8.5 respectively. This also complies with the restrictions set forth in the Eurotop manual. Small-scale

protective buildings need to consider the sea level rise in the next 50 years, that is, to 2065. Complex and difficult-to-renovate protective buildings need to consider the sea level rise in the next 100 years, that is, to 2100.

In the RCP2.6 emission scenario, until 2065, the average sea level rises to 0.24 meters, and the water level is high enough to cover the wall crest. When overtopping occurs, more than 5 m^3 of waves will be generated in an average of 20 seconds. When the sea level rises by 0.44m, which is about the sea level in 2100, the amount of surging is even more uncontrollable, with nearly 15 m^3 of surging every 20s. In this case, it is necessary to reconsider the design of the protective building, and reduce the wave overtopping by improving the crest or remodeling the building.
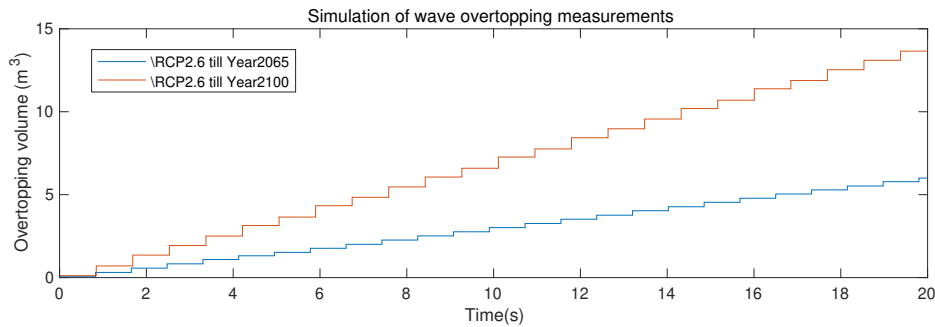

Figure 5.15: Overtopping volume comparison for RCP2.6 scenario

In the RCP4.5 emission scenario, until 2065, the average sea level rises to 0.26 meters, and the water level is high enough to cover the wall crest. When overtopping occurs, more than 5 m^3 of waves will be generated in an average of 20 seconds. This overtopping rate is similar to that of RCP2.6. When the sea level rises by 0.53m, which is about the sea level in 2100, the amount of wave overtopping is even more uncontrollable, with nearly 15 m^3 of overtopping volume every 15s. In this case, the protective building must be redesigned and constructed. Because the protective building at this time will not slow down the overtopping.

In the RCP6.0 emission scenario, until 2065, the average sea level rises to 0.2 meters, and the water level is high enough to cover the wall crest. When overtopping occurs, more than 5 m^3 of waves will be generated in an average of 20 seconds. This overtopping rate is similar to that of RCP2.6 and 4.5. When the sea level rises by 0.55m, which is about the sea level in 2100, the amount of wave overtopping is even more uncontrollable, with nearly 15 m^3 of water volume in every 15s. In this case, the protective building must be redesigned and constructed. The situation is similar to RCP4.5, because the protective building at this time will not have any mitigation effect on overtopping.
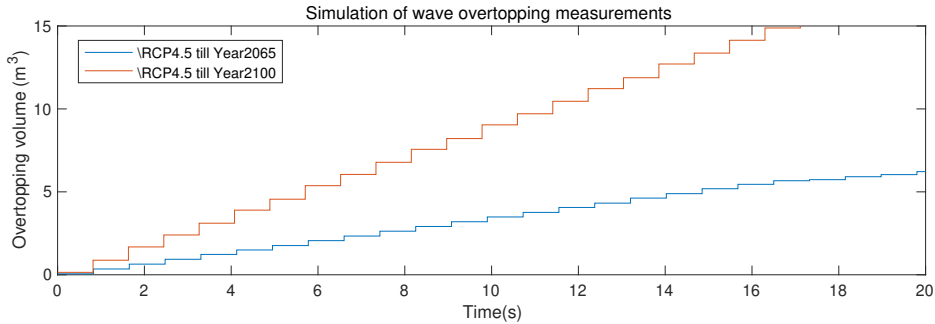
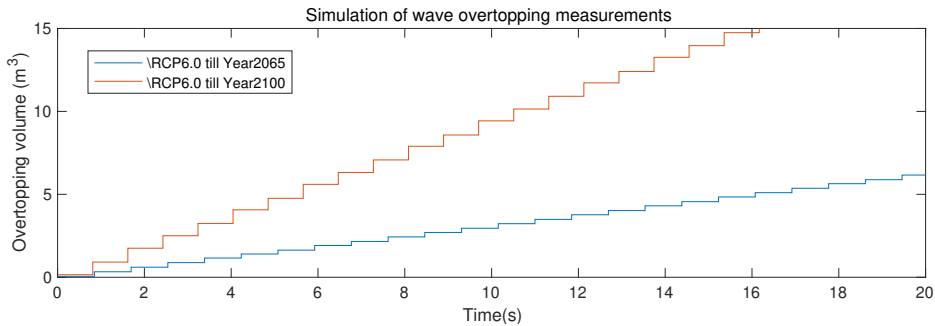Figure 5.16: Overtopping volume comparison for RCP4.5 scenario

Figure 5.17: Overtopping volume comparison for RCP6.0 scenario

In the RCP8.5 emission scenario, until 2065, the average sea level rises to 0.29 meters, and the water level is high enough to cover the wall crest. When overtopping occurs, more than 8 m^3 of waves will be generated in an average of 20 seconds. This overtopping rate is worse than RCP2.6 and 4.5. When the sea level rises by 0.74m, which is about the sea level in 2100, the amount of overtopping volume is the most uncontrollable, with nearly 15 m^3 of water volume every 10s. The protective building at this time will not slow down the overtopping.

Therefore, the defence structure in the design model is not able to function against the seal level rise in 2100, under all three RCPs emission scenarios. In this case, increasing the crest height of the defence structure or redesign the structural geometry is the rational solution to deal with sea level rise. At the same time, the simulation results under different emission scenarios indicate the significant influence of sea level rise on the wave overtopping. The severer RCP emission scenario applies, the higher wave overtopping rate is simulated. The calculated average of overtopping rate rises from 0.704 m^3/s (RCP2.6 in year 2100) to 1.438 m^3/s (RCP8.5 in year 2100). Therefore, it is indispensable for EurOtop Manual[40] to give design requirements related to sea level rise. Small and straightforward protective structures, such as earthen dike, can
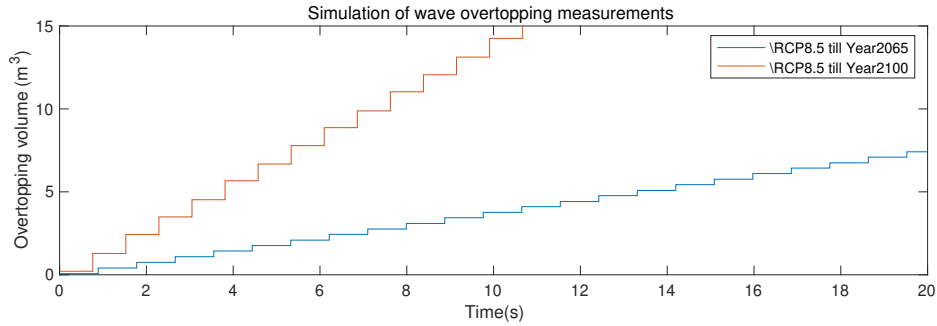
Figure 5.18: Overtopping volume comparison for RCP8.5 scenario

improve applicability by improving crest. Therefore, under different RCPs in 2065, maintenance can be carried out and reconstruct partially. Complex protective structures, such as concrete dike, need to be constructed in consideration of sea level rise in the next 100 years. Because this kind of complex structure or special material dike is not suitable for rebuild partially, under most of the sea level rise predictions given by the IPCC in 2100, defence structure without sea level design will be ineffectual. Therefore, follow Eurotop's The design requirements for sea level rise are reasonable and necessary.

Chapter 6

Discussion

This thesis applied REEF3D::SFLOW framework as a tool to simulate wave propagation on a complex coastal structure and calculate wave overtopping discharge based on simulation. The summarized contents are shown as follows:

- The thesis introduces the REEF3D model, including the governing equation, convective term, time step, dynamic boundary conditions, wave absorption method and so on.

- The related functions of REEF3D::SFLOW are used to simulate one-dimensional regular waves, two-dimensional regular waves, two-dimensional breaking wave, and the results are compared with theoretical values. The results prove that REEF3D::SFLOW is able to simulate two-dimensional numerical wave tank. The applications also prove the possibility to simulate a complex coastal system. Besides, this thesis simulates a large scale wave propagation with topography, proving the feasibility of REEF3D::SFLOW into practical application.

- By the simulation results of REEF3D::SFLOW, this thesis successfully calculates wave overtopping discharge on a complex structure. The comparison of simulation results and experimental measurement prove the validation of REEF3D::SFLOW on wave overtopping.

- This thesis studies the impact of sea level rise on wave overtopping rate by simulating overtopping discharge on the model structure in the next 100 years under the scenarios of RCP2.6, RCP4.5, RCP6.5 and RCP8.5. The predictions are identical to requirements in coastal defence structure design in EurOtop Manual.

The research in this thesis is of academic and practical values. However, several research topics are recommended to be carried out in the future researches due to the

time limit of the thesis. Some details need further research in the future: First, a more thorough grid convergence study needs to be performed for complex structures. Second, the differences between the simulated surface elevations and the experiment need to be further investigated. The more in-depth study on the effect of sea level rise on wave overtopping by the influence of the structure element shape and wave velocity distribution etc. is expected.

Bibliography

[1] M. S. Afzal. 3d numerical modelling of sediment transport under current and waves. Master's thesis, NTNU, 2013.

[2] A. Aggarwal, H. Bihs, S. Shirinov, and D. Myrhaug. Estimation of breaking wave properties and their interaction with a jacket structure. *Journal of Fluids and Structures*, 91:102722, 2019.

[3] N. Ahmad, H. Bihs, D. Myrhaug, A. Kamath, and Ø. A. Arntsen. Three-dimensional numerical modelling of wave-induced scour around piles in a side-by-side arrangement. *Coastal Engineering*, 138:132 – 151, 2018.

[4] N. Ahmad, H. Bihs, D. Myrhaug, A. Kamath, and Ø. A. Arntsen. Numerical modelling of pipeline scour under the combined action of waves and current with free-surface capturing. *Coastal Engineering*, 148:19 – 35, 2019.

[5] N. Ahmad, A. Kamath, and H. Bihs. 3D numerical modelling of scour around a jacket structure with dynamic free surface capturing. *Ocean Engineering*, 200:107104, 2020.

[6] M. Alagan Chella, H. Bihs, A. Kamath, D. Myrhaug, and Ø. A. Arntsen. Breaking Wave Interaction With a Group of Four Vertical Slender Cylinders in Two Square Arrangements. *Journal of Offshore Mechanics and Arctic Engineering*, 141(6), 05 2019.

[7] H. Bihs and A. Kamath. A combined level set/ghost cell immersed boundary representation for floating body simulations. *International Journal for Numerical Methods in Fluids*, 83(12):905–916, 2017.

[8] H. Bihs, A. Kamath, M. Alagan Chella, A. Aggarwal, and Ø. A. Arntsen. A new level set numerical wave tank with improved density interpolation for complex wave hydrodynamics. *Computers & Fluids*, 140(Supplement C):191 – 208, 2016.

[9] J. Bosboom and M. Stive. *Coastal Dynamics : Part 1 (version 2011-0.2)*, volume Part 1 (version 2011-0.2). VSSD, 2011. Lecture Notes CT4305.

[10] J. A. Church and N. J. White. Sea-level rise from the late 19th to the early 21st century. *Surveys in Geophysics*, 32(4-5):585–602, Mar 2011.

[11] P. G. DRAZIN. ON THE STABILITY OF CNOIDAL WAVES. *The Quarterly Journal of Mechanics and Applied Mathematics*, 30(1):91–105, 02 1977.

[12] J. D. Fenton. A high-order cnoidal wave theory. *Journal of Fluid Mechanics*, 94(1):129–161, 1979.

[13] T. O. Foundation. *OpenFOAM v8 User Guide*. The OpenFOAM Foundation, 2020.

[14] A. Harten and S. Efrony. A partition technique for the solution of potential flow problems by integral equation methods. *Journal of Computational Physics*, 27(1):71 – 87, 1978.

[15] C. Hirt and B. Nichols. Volume of fluid (vof) method for the dynamics of free boundaries. *Journal of Computational Physics*, 39(1):201 – 225, 1981.

[16] IPCC. *Climate Change 2013: The Physical Science Basis*. Contribution of Working Group I to the [[IPCC Fifth Assessment Report—Fifth Assessment Report]] of the Intergovernmental Panel on Climate Change. Cambridge University Press, Cambridge, United Kingdom and New York, NY, USA, 2013.

[17] IPCC. *Climate Change 2014: Impacts, Adaptation, and Vulnerability, Part A: Global and Sectoral Aspects*, chapter Chapter 5: Coastal Systems and Low-Lying Areas, pages 361–409. Contribution of Working Group II to the Fifth Assessment Report of the Intergovernmental Panel on Climate Change. Cambridge University Press, Cambridge, United Kingdom and New York, NY, USA, 2014.

[18] Y. Iwagaki, A. Shima, and M. Inoue. Effects of wave height and sea water level on wave overtopping and wave run-up. *Coastal Engineering in Japan*, 8(1):141–151, Dec 1965.

[19] A. Jeschke, G. K. Pedersen, S. Vater, and J. Behrens. Depth-averaged non-hydrostatic extension for shallow water equations with quadratic vertical pressure profile: equivalence to boussinesq-type equations. *International Journal for Numerical Methods in Fluids*, 84(10):569–583, 2017.

[20] G.-S. Jiang and C.-W. Shu. Efficient implementation of weighted eno schemes. *Journal of Computational Physics*, 126(1):202 – 228, 1996.

[21] S. Levitus, J. Antonov, and T. Boyer. Warming of the world ocean, 1955–2003. *Geophysical Research Letters*, 32(2), 2005.

[22] T. Lukovic. *Nautical Tourism*, page 116. CABI International, 2013.

[23] P. A. MADSEN, H. B. BINGHAM, and H. LIU. A new boussinesq method for fully nonlinear waves from shallow to deep water. *Journal of Fluid Mechanics*, 462:1–30, 2002.

[24] P. A. Madsen and H. A. Schäffer. Higher-order boussinesq-type equations for surface gravity waves: Derivation andanalysis. *Philosophical Transactions: Mathematical, Physical and Engineering Sciences*, 356(1749):3123–3184, 12 1998.

[25] T. Martin, A. Kamath, and H. Bihs. Modeling and Simulation of Moored-Floating Structures Using the Tension Element Method. *Journal of Offshore Mechanics and Arctic Engineering*, 142(1), 08 2019.

[26] J. B. Martin S. Aln. The fenics project version 1.5. *Archive of Numerical Software*, 3(100):9–23, 2015.

[27] B. L. Mehaute. *An Introduction to Hydrodynamics and Water Waves*. Springer-Verlag Berlin Heidelberg, 1976.

[28] E. D. C. Michael Selwyn Longuet-Higgins. The deformation of steep surface waves on water - i. a numerical method of computation. *Proceedings of the Royal Society of London. A. Mathematical and Physical Sciences*, 350(1660):1–26, Jul 1976.

[29] M. Miche. Mouvements ondulatoires de la mer en profondeur constante ou décroissante. *École nationale des ponts et chaussées*, 1944.

[30] A. Mokos, R. Carmigniani, A. Leroy, and D. Violeau. Simulating wave overtopping on a complex coastal structure using sph. *Journal of Applied Water Engineering and Research*, 8(1):55–65, 2020.

[31] A. W. Nobuhisa Kobayashi. Wave overtopping on coastal structures. *Journal of Waterway, Port, Coastal, and Ocean Engineering*, 115(2):235–251, 1989.

[32] X.-D. L. S. Osher and T. Chan. Weighted essentially non-oscillatory schemes. *Journal of Computational Physics*, 115(1):200–212, 1994.

[33] M. Owen. Design of seawalls allowing for wave overtopping. *Hydraulics Research Wallingford,England*, 1980.

[34] T. Prime, J. M. Brown, and A. J. Plater. Physical and economic impacts of sea-level rise and low probability flooding events on coastal communities. *PLOS ONE*, 10(2):e0117030, Feb 2015.

[35] B. E. Rapp. Chapter 3 - engineering mathematics. In B. E. Rapp, editor, *Microfluidics: Modelling, Mechanics and Mathematics*, Micro and Nano Technologies, pages 21 – 50. Elsevier, Oxford, 2017.

[36] T. Saville. *Laboratory data on wave run-up and overtopping on shore structures*. U.S. Beach Erosion Board, [Washington D.C.], 1955.

[37] C.-W. Shu and S. Osher. Efficient implementation of essentially non-oscillatory shock-capturing schemes. *Journal of Computational Physics*, 77(2):439 – 471, 1988.

[38] A. S. M. Soliman. Numerical study of irregular wave overtopping and overflow. Master's thesis, University of Nottingham, 2003.

[39] J. van der Meer and H. Janssen. Wave run-up and wave overtopping at dikes. *Wave Forces on inclined and Vertical Structure ASCE*, pages 1–27, 01 1995.

[40] J. W. van der Meer, N. Allsop, T. Bruce, J. De Rouck, A. Kortenhaus, T. Pullen, H. Schüttrumpf, P. Troch, and B. Zanuttigh. *EurOtop: Manual on wave overtopping of sea defences and related sturctures : an overtopping manual largely based on European research, but for worlwide application*, 2016.

[41] P. Wang, Y. Yao, and M. P. Tulin. An efficient numerical tank for non-linear water waves, based on the multi-subdomain approach with bem. *International Journal for Numerical Methods in Fluids*, 20(12):1315–1336, 1995.

[42] W. Wang, T. Martin, A. Kamath, and H. Bihs. An improved depth-averaged nonhydrostatic shallow water model with quadratic pressure approximation. *International Journal for Numerical Methods in Fluids*, 92(8):803–824, 2020.

[43] J. R. Weggel. Wave overtopping equation. *Coastal Engineering 1976*, Nov 1977.

[44] Yang. *Image2Data Overview*. Matlab, 4 2020.